The Department of Geodesy and Geoinformatics

Stuttgart University
2015

Dear friends and colleagues,

It is our great pleasure to present to you this annual report[1] on the 2015 activities and academic highlights of the Department of Geodesy & Geoinformatics of the University of Stuttgart. The Department consists of the four institutes:

- ▷ Institute of Geodesy (GIS),
- ▷ Institute of Photogrammetry (ifp),
- ▷ Institute of Navigation (INS),
- ▷ Institute of Engineering Geodesy (IIGS),

and is part of the Faculty of Aerospace Engineering and Geodesy.

Research

This annual report documents our research contributions in many diverse fields of Geodesy and Geoinformatics: from satellite and physical geodesy through navigation, remote sensing, engineering surveying and telematics to photogrammetry, geographical information systems and location based services. Detailed information on projects and research output can be found in the following individual institutes' sections.

Teaching

We were able to welcome 69 new BSc students in winter-term 2014/2015. The first BSc students graduated at the end of 2013. Until the end of 2015 we had in total 53 BSc graduates. The MSc program for Geodesy and Geoinformatik started with the winter-term 2012. Currently 36 students are taking part in this Master of Science program and we have already 14 MSc graduates. The Diploma program is slowly being phased out. Total enrolment, in both the BSc, MSc and the Diploma programs, is increasing an amounts to 225 students. Please visit our website *www.geodaesie.uni-stuttgart.de* for additional information on the programs.

In its 10th year of existence, our international MSc program *Geomatics Engineering* (GeoEngine) enjoys a gratifying demand. We register an enrolment of 32 students. We attract the GeoEngine student population from such diverse countries as China, Palestine, Mongolia, Iran, Pakistan, India, Indonesia, Thailand, Cyprus, Colombia, Venezuela, Uzbekistan, Taiwan, Romania, Poland, Syria, and Russia. Please visit *www.geoengine.uni-stuttgart.de* for more information.

---

[1]A version with colour graphics is downloadable from
http://www.ifp.uni-stuttgart.de/publications/jahresberichte/jahresbericht.html

Awards and scholarships

We want to express our gratitude to our friends and sponsors, most notably

▷ Verein Freunde des Studienganges Geodäsie und Geoinformatik an der Universität Stuttgart e.V. (F2GeoS),

▷ Microsoft company Vexcel Imaging GmbH,

▷ Ingenieur-Gesellschaft für Interfaces mbH (IGI),

▷ DVW Landesverein Baden-Württemberg,

who support our programs and our students with scholarships, awards and travel support.

Below is the list of the recipients of the 2014/15 awards and scholarships. The criterion for all prizes is academic performance; for some prizes GPA-based, for other prizes based on thesis work. Congratulations to all recipients!

Wolfgang Keller
Associate Dean (Academic)
wolfgang.keller@gis.uni-stuttgart.de

Award	Recipient	Sponsor	Programme
Karl-Ramsayer Preis	D. Xie	Department of Geodesy & Geoinformatics	Geodesy & Geo-informatics
BSc/MSc Thesis Award	L. Diemer	F2GeoS	Geodesy & Geo-informatics
MS Photogrammetry / Vexcel Imaging Scholarship	S. Gu B. Koirala Y. Pang	MS Photogrammetry / Vexcel Imaging	GEOENGINE
matching funds	O. B. Agyei Z. Li Z. Liu A. M. Moanta Y. Song	DAAD	GEOENGINE

Institute for Engineering Geodesy

Geschwister-Scholl-Str. 24D, D-70174 Stuttgart,
Tel.: +49 711 685 84041, Fax: +49 711 685 84044
e-mail: Sekretariat@ingeo.uni-stuttgart.de or
firstname.secondname@ingeo.uni-stuttgart.de
url: http://www.uni-stuttgart.de/ingeo/

Head of Institute

Prof. Dr.-Ing. habil. Volker Schwieger

Secretary

Elke Rawe
Ute Schinzel

Emeritus

Prof. Dr.-Ing. Dr.sc.techn.h.c. Dr.h.c. Klaus Linkwitz

Scientific Staff

M.Sc. Ashraf Abdallah	GNSS Positioning
M.Sc. Bara' Al-Mistarehi	Construction Process
M.Sc. Aiham Hassan	Monitoring
Dipl.-Ing. Stephanie Kauker	Monitoring
Dipl.-Ing. Otto Lerke	Machine Guidance
M.Sc. Xiaojing Lin (until 28.02.2015)	Machine Guidance
Dr.-Ing. Martin Metzner	Engineering Geodesy
Dipl.-Ing. Annette Scheider	Kinematic Positioning
M.Sc. Pham Trung Dung	Kinematic Positioning
M.Sc. Annette Schmitt	Multi-Sensor-Systems
M.Sc. Rainer Schützle	Location Referencing
M.Sc. Jinyue Wang (since 01.06.2015)	Map Matching
Dipl.-Ing. Li Zhang	Monitoring
Dipl.-Ing. Bimin Zheng (until 31.03.2015)	Monitoring

Technical Staff

Andreas Kanzler
Martin Knihs
Lars Plate

External Teaching Staff

Dipl.-Ing. Jürgen Eisenmann	Landratsamt Ludwigsburg - Fachbereich Vermessung
Dipl.-Ing. Christian Helfert	Fachdienstleiter Flurneuordnung im Landkreis Biberach
Dipl.-Math. Ulrich Völter	Geschäftsführer der Fa. Intermetric
Dr.-Ing. Thomas Wiltschko	Daimler AG, Mercedes-Benz Cars; Research and Development

General View

The Institute of Engineering Geodesy (IIGS) is directed by Prof. Dr.-Ing. habil. Volker Schwieger. It is part of the Faculty 6 „Aerospace Engineering and Geodesy" within the University of Stuttgart. Prof. Schwieger holds the chair in „Engineering Geodesy and Geodetic Measurements". In 2012 he was elected Vice Dean of Faculty 6.

In addition to being a member of Faculty 6, Prof. Schwieger is co-opted to Faculty 2 „Civil and Environmental Engineering". Furthermore, IIGS is involved in the Center for Transportation Research of the University of Stuttgart (FOVUS). Prof. Schwieger presently acts as speaker of FOVUS. So, IIGS actively continues the close collaboration with all institutes in the field of transportation, especially with those belonging to Faculty 2.

Since 2011 he is full member of the German Geodetic Commission (Deutsche Geodätische Kommission - DGK). Furthermore, Prof. Schwieger is a member of the section „Engineering Geodesy" within the DGK. He is head of the DVW working group 3 „Measurement Techniques and Systems" and chairman of the FIG Commission 5 „Positioning and Measurements" for the period 2015-2018.

The institute's main tasks in education focus on geodetic and industrial measurement techniques, kinematic positioning and multi-sensor systems, statistics and error theory, engineering geodesy and monitoring, GIS-based data acquisition, and transport telematics. Here, the institute is responsible for the above-mentioned fields within the curricula of „Geodesy and Geoinformatics" (Master and Bachelor courses of study) as well as for „GEOENGINE" (Master for Geomatics Engineering in English). In addition, the IIGS provides several courses in German for the curricula of „Aerospace Engineering" (Bachelor and Master), „Civil Engineering" (Bachelor and Master), „Transport Engineering" (Bachelor and Master) and „Technique and Economy of Real Estate" (Bachelor). Furthermore, lectures are given in English to students within the master course „Infrastructure Planning". Finally, eLearning modules are applied in different curricula.

The current research and project work of the institute is expressed in the course contents, thus always presenting the actual state-of-the-art to the students. As a benefit of this, student research projects and theses are often implemented in close cooperation with the industry and external research partners. The main research focuses on kinematic and static positioning, analysis of engineering surveying processes and construction processes, machine guidance, monitoring, transport and aviation telematics, process and quality modeling. The daily work is characterized by intensive co-operation with other engineering disciplines, especially with traffic engineering, civil engineering, architecture and aerospace engineering.

Research and Development

Improving the Quality of Low-Cost GPS Receiver Data Using Spatial Correlations

The investigations on low-cost single frequency GPS receivers at the Institute of Engineering Geodesy (IIGS) show that u-blox LEA-6T GPS receivers combined with Trimble Bullet III GPS antennas containing self-constructed L1-optimized choke rings can already obtain an accuracy in the range of millimeters which meets the requirements of geodetic precise monitoring applications. However, the quality (accuracy and reliability) of low-cost GPS receiver data, particularly in shadowing environment, should still be improved, since the multipath effects are the major error for the short baselines.

For this purpose, as shown in Figure 1, a 3 x 3 antenna array was set up next to the metal wall on the roof of the IIGS building, with a distance between two antennas of 0.5 m, so the antenna array has an extension of 1 m x 1 m. Static measurement was carried out for 26 days (from 3 March to 1 April 2014). The GPS raw data were recorded from the 9 receivers at 1 Hz, stored on a PC, evaluated and post-processed. One SAPOS station is only about 500 m away from the test field. This station is taken as reference station and the 9 stations in the test field are taken as rover stations for processing the baselines, so that 9 baselines can be obtained.
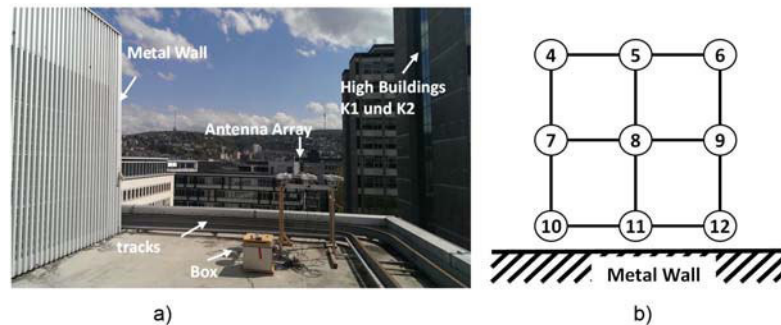

Figure 1: Photos of test field with antenna array a) and Antenna number b).

The time series of three-dimensional coordinates of the GPS receivers were analysed. The coordinate residuals contain both non-correlating and correlating errors. Only the correlated errors are of interest. The non-correlating errors are reduced by using the moving average filter. By analysing the coordinates, it is noticed that the coordinates often contain oscillations with periods of 30 to 40 seconds. These periods are probably caused by the multipath effects from the two high buildings. These periods are so short that they are not really of interest for monitoring. For this reason, 40 seconds are chosen as window size of the moving average. In Figure 2 the smoothed baselines s-a4 and s-a5 and their cross-correlation functions of the first 15-minutes block are shown.

It can be found out that their residuals can be quite similar (compare east and height component) but sometimes are not (compare north component), and there are time shifts between their errors. That means that similar errors can be present in baseline s-a4 as well as in baseline s-a5 with a time shift.
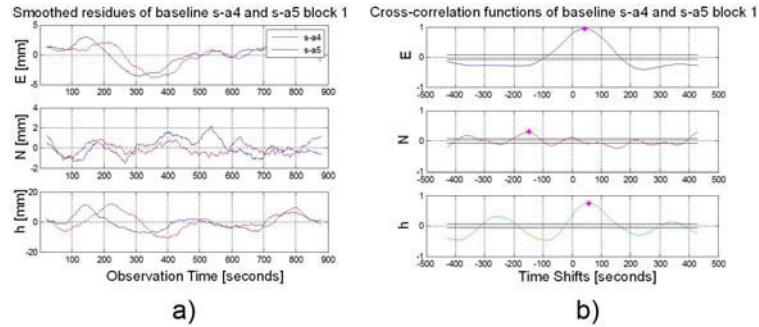

Figure 2: a) Smoothed baselines s-a4 and s-a5 and b) Cross-correlation functions between them.

Block 1 is just an example, the time shifts vary from block to block and can be positive or negative as well as zero. The correlations of each coordinate component also vary from block to block. They depend on the geometry of satellite-antenna-reflectors.

Thus, the idea of the algorithm is that the coordinates of one station (station A) can be corrected using the spatial correlations of coordinates of an adjoined station (station B), so that the accuracy and reliability of the GPS measurement is improved:

$$kr_{\overline{SA},j,q}(t) = k_{\overline{SA},j,q}(t) - m_{j,q} \cdot k_{\overline{SB},j,q}(t + \Delta t). \tag{1}$$

As shown in Equation (1), $k_{\overline{SA},j,q}(t)$ and $k_{\overline{SB},j,q}(t)$ are residuals of two baselines in j-component (j=E,N,h) and q block (q=1,2,...96). These residuals are free from the mean value. The geometric relationship between the stations S, A, B is used to correct part of the errors from the GPS processing. This will not be explained here. It can be derived from the cross-correlation function that

the two residuals $k_{\overline{SA},j,q}(t)$ and $k_{\overline{SB},j,q}(t)$ have the maximum correlation at time shift Δt. $k_{\overline{SB},j,q}(t)$ will be taken and shifted about Δt, so that we can achieve $k_{\overline{SB},j,q}(t+\Delta t)$. It is assumed that there is scale $m_{j,q}$ between $k_{\overline{SA},j,q}(t)$ and $k_{\overline{SB},j,q}(t+\Delta t)$, so $k_{\overline{SB},j,q}(t+\Delta t)$ will be scaled and used to correct the $k_{\overline{SA},j,q}(t)$, therefore the corrected residuals for the baseline SA is $kr_{\overline{SA},j,q}(t)$. The maximum of the cross-correlation function can be taken as scale $m_{j,q}$, or $m_{j,q}$ can be estimated by adjustment. The scale calculated by adjustment provides better results, since the scale larger than 1 (compare Equation (1)) is a possible solution for some cases. This cannot be delivered by correlation functions.

For example, a4 and a5 are regarded as station A and B. The residuals of baseline s-a5 can be taken to correct the residuals of baseline s-a4. In Figure 3a) the residuals of baseline s-a5 are shifted by Δt and compared with the baseline s-a4. The residuals of baseline s-a4 $k_{\overline{sa4},j,q}(t)$ and the corrected s-a4 $kr_{\overline{sa4},j,q}(t)$ using $k_{\overline{sa5},j,q}(t)$ according to Equation (1) are shown in Figure 3b). The performance of this algorithm is dependent on the spatial correlation. In Figure 3b) it can be seen that oscillations in the east and height component are significantly suppressed, since the correlations between these two components are very high. The correction does not work well in the north component, since the correlation is quite low.
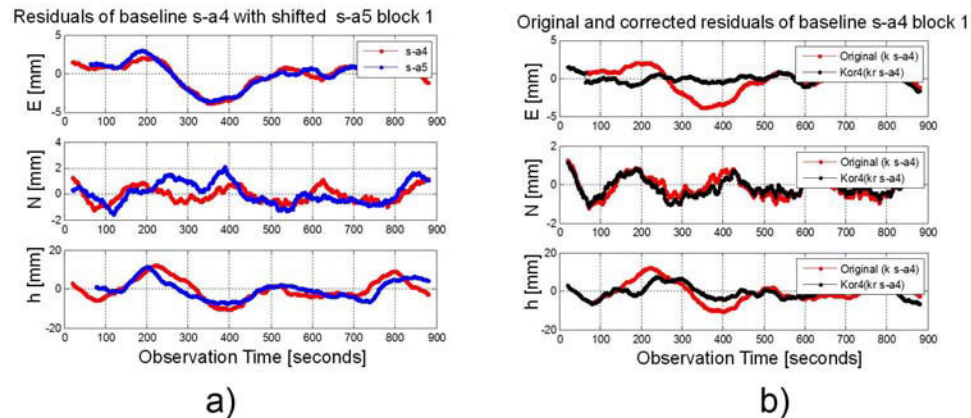

Figure 3: a) Residuals of baseline s-a4 with shifted s-a5 and b) original and the corrected baseline s-a4.

The spatial correlation varies from time to time. Thus, the performance of the algorithm is evaluated for all 96 blocks. The standard deviations of baseline s-a4 can be improved on average by about 50% by using the spatial correlation with baseline s-a5.

Effect of Satellite Clocks on Kinematic PPP solution for the Hydrographic Survey

Since the GNSS technique provides the position of objects with high accuracy, this technique has become one of the most important techniques to obtain hydrographic information. Over the last two decades, the precise point positioning (PPP) technique, which uses only a single receiver has gained an increase of interest. To obtain the centimeter accuracy level, a dual frequency GNSS instrument is required. The sampling rate of the satellite clocks affects the accuracy of kinematic PPP solution. The precise satellite orbits and clocks may be provided from the International GNSS Service (IGS). A comparison between the Bernese GNSS V. 5.2 software and CSRS-PPP online service has been carried through. During the processing, the satellite clocks provided by IGS with a sampling rate of 30 seconds were used.

In order to identify the accuracy of kinematic PPP solution for hydrographic survey, three kinematic trajectories were observed on the Rhine River, Duisburg, Germany as a part of project „HydrOs - Integrated Hydrographical Positioning System". This project is launched in co-operation between the department M5 (Geodesy) of the German Federal Institute of Hydrology (BfG) and the Institute of Engineering Geodesy at the University of Stuttgart (IIGS). An antenna of LEIAX1203+GNSS and a receiver LEICA GX1230+GNSS were located on the surveying vessel (Mercator) to collect the GNSS data. Figure 4 presents the surveying vessel and the GNSS antenna over it.

Figure 4: „Mercator" observation vessel for the measurement data (left figure); GPS antenna over the vessel (right figure).

Table 1 presents the statistical results, Root mean square (RMS) as well as standard deviation σ, obtained from Bernese GNSS software and CSRS-PPP online service. These results are calculated relative to the double-difference solution from Bernese software.

As shown in Figure 5, Bernese solution delivers in average a standard deviation of 7 cm for the horizontal components, and 12 cm for vertical components. CSRS-PPP online service provides a better solution than that obtained by Bernese software. It shows in average a standard deviation of 6 cm in all components.

		TRAJ1			TRAJ2			TRAJ3		
		East	North	height	East	North	height	East	North	height
Bernese GNSS	RMS [m]	0.081	0.104	0.010	0.10	0.09	0.113	0.050	0.052	0.149
	σ [m]	0.081	0.096	0.096	0.068	0.075	0.107	0.050	0.052	0.144
CSRS-PPP	RMS [m]	0.182	0.114	0.068	0.082	0.082	0.087	0.023	0.026	0.041
	σ [m]	0.098	0.104	0.063	0.066	0.072	0.087	0.022	0.022	0.033

Table 1: Statistical results from Bernese GNSS software and CSRS-PPP online service.
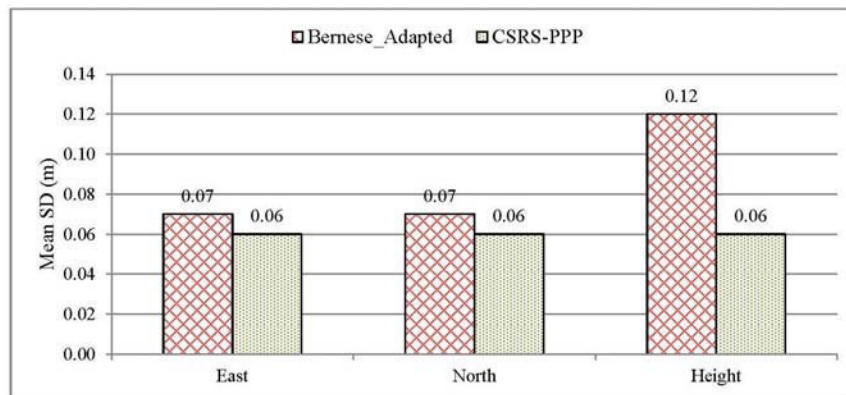
Figure 5: Mean SD for Bernese GNSS and CSRS-PPP online service.

Integration of additional sensors in the HydrOs system

The system HydrOs includes a multi-sensor system and an evaluation software to determine continuously the position and the spatial orientation of a surveying vessel on inland waterways. This system is able to bridge gaps in GNSS-RTK measurements so that reliable coordinates are also available in GNSS shadowed areas or in areas without reception of a GNSS reference service (e. g. SAPOS®). This system has been developed by IIGS and the Federal Institute of Hydrology (BfG).

Now new optional components are integrated into the system and analysed. Next to additional filtering algorithms (software components) also new sensors are tested: A camera is mounted on the vessel and takes images of the riverside in short time intervals. These images are evaluated with Agisoft PhotoScan to estimate the exterior orientation of each image. If known points along the riverside or some known camera positions are used to georeference the data, the complete trajectory of camera positions will be determined in the UTM coordinate system. This information is integrated as additional position observation into the HydrOs software. Thus, coordinates should be available also in parts of the trajectory which do not contain any valid GNSS positions.

Because only reliable coordinates can be used, the resulting camera coordinates must be determined carefully: Poor environmental conditions may cause unreliable camera coordinates. According to the time of capturing and the shape of the river, the light conditions change suddenly and can be challenging (shadowed areas, sun shines directly into the objective lens). Low image overlaps may also be a problem. Besides, the timing component must be considered: To improve the results of the Extended Kalman Filter (EKF) in the HydrOs software, each camera position must have a precise time stamp.

To test the performance of the system, measurement data was captured on the river Rhine close to Duisburg-Homberg (Figure 6). In this area, the vessel was driving approximately in north-south direction.

Figure 6: Photo of the riverside in Duisburg-Homberg.

By integrating these data (Figure 7) into the HydrOs software, the estimated coordinates can be improved. For this reason, the EKF results are compared to the results of the default HydrOs sensor configuration without camera. After a simulated gap of approx. 1 minute in the GNSS measurement data, the maximal deviation in the transversal direction (Easting) of the trajectory is decreased to 55.7 % and 34.5 % respectively.
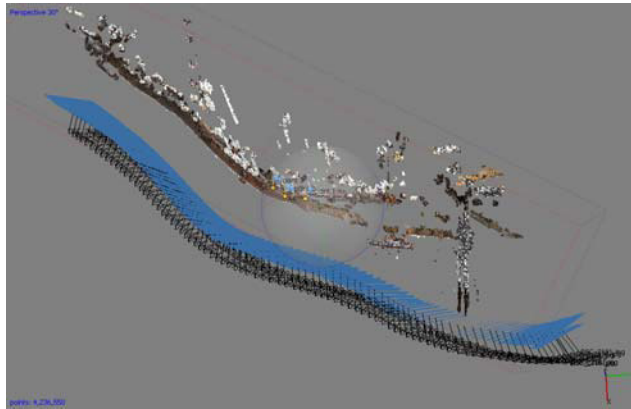
Figure 7: Trajectory of camera positions, evaluated with Agisoft PhotoScan.

Construction of a Synthetic Covariance Matrix for Terrestrial Laserscanning

This work is part of the project IMKAD, which is funded by the Deutsche Forschungsmeinschaft (DFG) and realized in cooperation of the Institute of Engineering Geodesy, University of Stuttgart, with the Department of Geodesy and Geoinformation, Vienna University of Technology.

Considering the correlations within a terrestrial laserscanning point cloud requires a synthetic covariance matrix. This matrix contains variances and co-variances computed from the main influences on terrestrial laserscanning measurements. Building a synthetic covariance matrix is based on the elementary error model. In order to construct a synthetic covariance matrix, all considered error sources should be classified into different groups regarding their type of correlation. A distinction is made between non-correlating, functional correlating and stochastical correlating groups, in which each group is expressed by one variance/co-variance matrix.

Applying the elementary error model on terrestrial laserscanning measurements requires the determination of the main impacts. For this reason, it is assumed that the functionality of a terrestrial laser scanner is mainly similar to the one of a tachymeter. Hereby, most of the instrumental impacts, such as range error, collimation axis error and vertical index error are classified to the functional group. Range noise and angular noise, on the other hand, define non-correlating errors. Moreover, the atmospheric impacts and object-based impacts are classified to the stochastic correlating group. Nevertheless, the atmospheric impacts are modeled functionally at the time of writing due to homogeneous laboratory measurement conditions. Furthermore, object-based impacts like color, penetration depth, reflectivity and roughness are combined to one influencing parameter since it has not been possible to separate them yet. Another essential impact is caused by the angle of incidence between the laser beam hitting the object's surface and its normal vector of the same point. Next, the functional relations between the elementary errors and the observations

are necessary, in order to calculate numerical influences, variances and co-variances respectively. Summing up all variance/co-variance matrices results in the synthetic covariance matrix Σ_{ll}, as shown below in Equation (2):

$$\Sigma_{ll} = \sum_{k=1}^{p} D_k * \Sigma_{\delta\delta,k} * D_k^T + F * \Sigma_{\xi\xi} * F^T + \sum_{h=1}^{q} G_h + \Sigma_{\gamma\gamma,h} * G_h^T \tag{2}$$

By means of this, an error of position regarding each point within the point cloud can be calculated. Furthermore, the correlation matrix can be determined by standardization of the synthetic covariance matrix (see Equation (3)).

$$R_{ll} = \frac{1}{\sqrt{diag(\Sigma_{ll})}} * \Sigma_{ll} * \frac{1}{\sqrt{diag(\Sigma_{ll})}} \tag{3}$$

Its structure, which is equal to the one of Σ_{ll}, provides the computation of correlations of each coordinate axis. Figure 8 shows first results of a modelled rectangle with the size of 30 cm x 25 cm regarding spatial correlations of the collimation axis. Due to the spot size of about 9 mm of the laser beam at a distance of 10 m the chosen point distance of 12 mm for modelling is justified. As result, the error of position reaches 4 mm over the entire area. In addition, the small size of the grid causes high spatial correlations regarding the collimation axis.
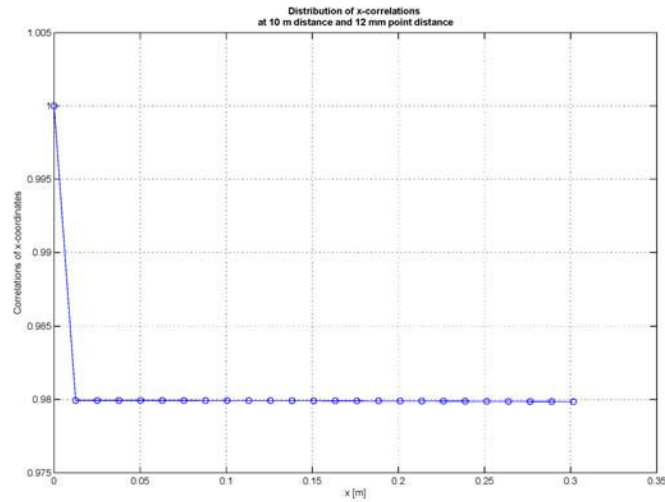

Figure 8: Correlations of x-coordinates depending on their distances to each other.

In future work, temporal correlations as well as optimizing the atmospheric model might be considered. Moreover, evaluating the synthetic covariance matrix by multiple scans is necessary in order to provide temporal correlations between observations. Furthermore, modelling real atmospheric impacts must be implemented by considering test bodies such as barrages and dams.

Comparison of Extended Kalman Filter, Unscented Kalman Filter and Particle Filter focusing on simulation of vehicle positioning

A comparison of three estimation algorithms including Extended Kalman filter (EKF), Unscented Kalman filter (UKF) and Particle filter (PF) is performed in term of accuracy and computational time (Table 2). The root mean square error (RMSE) is determined from estimated value and true value for all trajectory points as:

$$\text{RMSE} = \sqrt{\frac{\sum_{i=1}^{N}((X_{true,i} - X_{est,i})^2 + (Y_{true,i} - Y_{est,i})^2}{N}} \tag{4}$$

where X_{true}, Y_{true}: positions of the true trajectory
X_{est}, Y_{test}: estimated positions of EKF, UKF, and PF
N: the number of epochs.

PF		UKF	EKF
Number of Particles	Second		
100	2		
200	4	2×10^{-2} second	3×10^{-3} second
500	9		
1,000	18		

Table 2: Execution time of filtering algorithms using Matlab R2014 running on a standard PC with a 2.66GHz Intel Dual Core processor and 4GB RAM.

The linear model is defined by a linear predicted model and a linear measurement model. The linear predicted model is based on straight line function by varying the positions and the velocity. The linear measurement model is a function of observed positions.

A non-linear model consists of a circle line function for predicted models by varying the positions, the angle, the velocity and the different direction and the non-linear measurement model established by distance and horizontal angle of measurements.

From the simulation results, the performance of the accuracy and the computational time can be summarized as
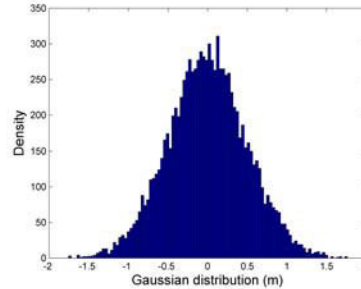
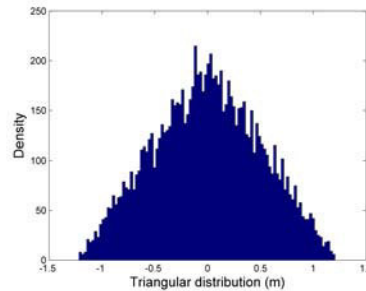*Figure 9: Histogram of Gaussian noise with the standard deviations of 0.5 m.*

Figure 10: Histogram of non-Gaussian noise using triangle distribution with the standard deviations of 0.5 m.

▷ Performance of the accuracy: For the linear estimation, the estimated results of three filtering algorithms are comparable with Gaussian noise (see Figure 9). In case of non-Gaussian noise (Figure 10), the best solution in term of accuracy belongs to PF. Two remaining algorithms are approximately equivalent. For the nonlinear estimation, the PF algorithm is the best solution with both Gaussian noise and non-Gaussian noise, especially to larger measurement standard deviation. UKF and EKF bring results with equivalent accuracy.

▷ Performance of the computational time: EKF is the fastest method and followed by UKF. The burden of computational time is due to the large required number of particles, which becomes the main drawback of PF.

For the linear model with Gaussian and non-Gaussian noise, EKF and UKF are suitable methods both in terms of accuracy and computational time. In contrast, PF is an effective method in terms of accuracy according to the nonlinear model (Figue 11).
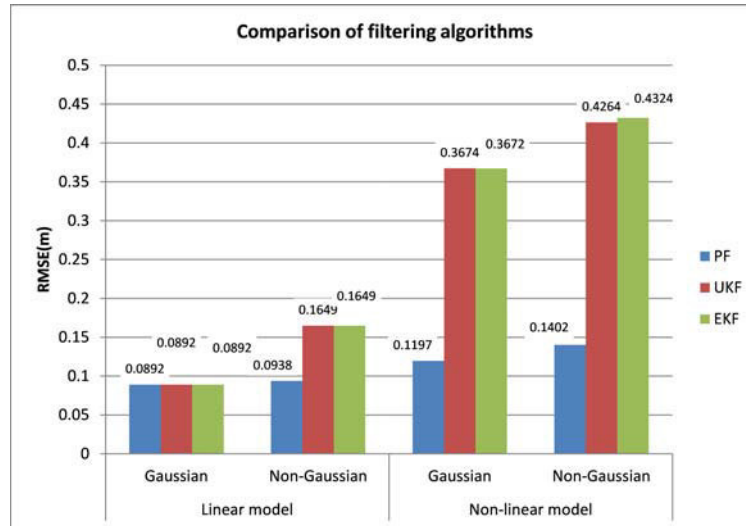
Figure 11: Comparison of the results of Gaussian and non-Gaussian distribution for the linear and non-linear models using the same standard deviations of 0.5 m.

Construction Machine Simulator - Control of a Model Dozer

The IIGS construction machine simulator was developed to test and evaluate different sensors, filter and control algorithms. In the recent configuration the simulator comprises a model dozer, in the scale of 1:14, a Leica TCRP 1201 tachymeter as positioning sensor, a control computer and an A/D converter (Figure 12).

The following new features have been implemented:

(a) New suitable set of PID controller parameters for the lateral control algorithm
(b) Longtidual control/speed control algorithm with an optionally selectable driving program
(c) Tool control

The description is split up into two thematic parts: the drive control including the features (a) and (b) and the tool control (feature (c)).

Drive Control

In previous works, a lateral control of a crawler model was implemented, allowing the vehicle to move automatically on a predefined trajectory. This is realized by different controllers, namely 2-point-, 3-point-, PID- and Fuzzy-controller. Due to the fact that a new crawler vehicle has been integrated into the simulator, new appropriate parameters for the PID controller had to be found.
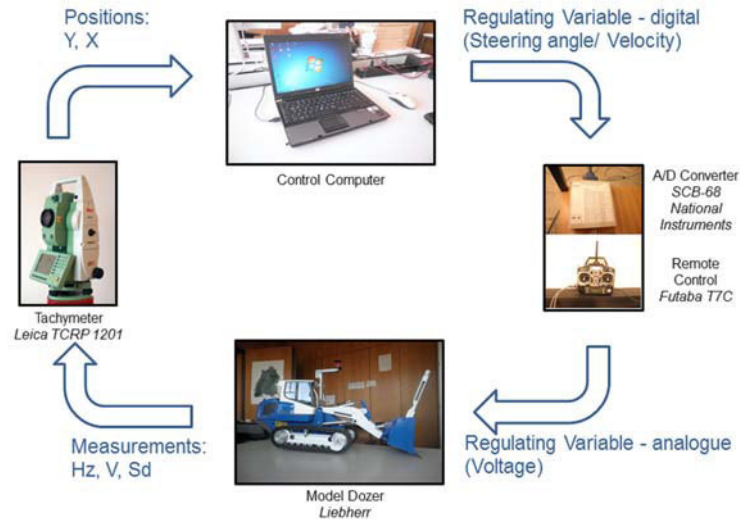
Figure 12: Hardware Components of the Recent Simulator Configuration.

Figure 13 shows the impact of different PID parameter settings on the driving behaviour of the crawler. The following new PID parameters for the lateral control could be derived from test drive analyses:

Proportional gain: K_P = 100,
Integral gain: K_I = 25,
Differential gain: K_D = 30.9.

Additionally, a speed control algorithm, as well based on a PID controller, was integrated into the control program. Two functions have been included. The first function allows the user to choose a desired moving velocity. Consequently the vehicle moves constantly with the set speed along the reference trajectory. It has the ability to keep constant speed even in critical parts of the trajectory, e.g. curves. This function is extended by an optionally selectable driving program. The driving program is geometry based and allows the user to set speed and the desired number of laps. After passing the set number of laps, it stops automatically at a defined end position. Thereby the acceleration and deceleration sequences are performed gradually, allowing smooth starts and stops.
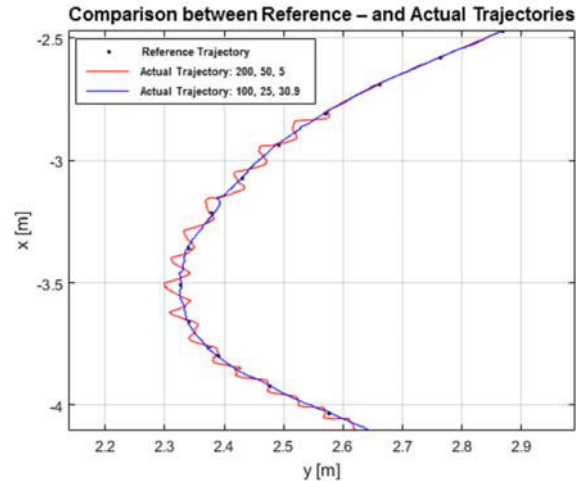
Figure 13: Impact of PID Controller Parameter Settings on the Driving Behaviour

For future works new transfer functions should be found to improve lateral and longitudinal guidance behaviour. For this, several calibration campaigns are planned.

Tool Control

The combination of a crawler chassis and the specific tool allows performing levelling works or loading processes. The focus of the recent report is on the levelling works.

The aim of levelling work is to produce a predefined plane or level for the following construction processes. This might be an area with equally distributed heights or a route or part of a route with differently distributed heights, e.g. slopes or ramps. Therefore the machine has to keep the working tool in a predefined height and tilt position.

The investigated tool consists of a cantilever arm and a bucket, assembled on the tip of the cantilever arm. The cantilever arm is mounted to the frame by two swivel joints. These joints act concurrently as arm's pivots (Figure 14). By performing rotational movements around the pivots the arm can be lifted and lowered. The bucket is attached to the tip of the arm by two further swivel joints. This configuration allows rotational movements (tilts) of the bucket around these joints. Each of the components is driven by a separate hydraulic circuit. Both hydraulic circuits are supplied by a single hydraulic pump.

Two sensors are fused to achieve control of the tool. For the control of the cantilever arm a tachymeter-reflector combination is used on the sensor side. The arm is controlled within a closed-loop system by the use of a PID controller. The bucket's control is realized by the attachment and
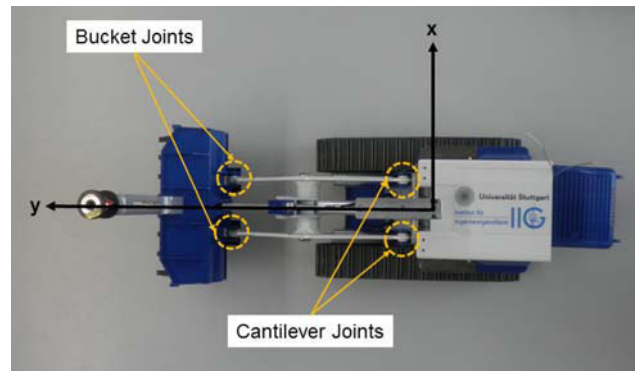
Figure 14: Position of the Swivel Joints (Top View).

alignment of an inertial measurement unit (IMU) alongside of the bucket. Therefore a second closed-loop-system is implemented. The control and regulation is realized by a 3-point controller. In this context, an important decision had to be made regarding the selection of the appropriate closed-loop controlled variable $y(t)$. It could be stated that incremental measurement techniques are not suitable for this specific kind of problem, because any kind of movement, coming from the chassis or the cantilever arm, is detected and integrated by the incremental sensor. Hence, the ability to state whether the movement is performed by the bucket, by the vehicles or by its components, is not given. Based on these facts the decision fell on an absolute measurement value. The „Microstrain 3DM-GX2" IMU is able to indicate the Euler angles. These 3 angles are defined as „Roll", „Pitch" and „Yaw". Regarding the tilt movement of the bucket the decision was made to use the „Pitch" information as controlled variable $y(t)$.

In the next steps the tachymeter-reflector combination is to be replaced by an alternative measurement technique, e.g. sonic sensor, to avoid negative effects of the prism position on the drive control. Furthermore an appropriate transfer function is to be found to describe the cantilever movement mathematically.

An Approach for Automated Detection and Classification of Pavement Crack

Considerable developments and improvements have been made in the field of automated crack detection in the last years. Digital image processing techniques for crack detection are already widely adapted on large highways maintenance projects. Complete automated crack detection is only realized for continuous pavement images series by commercial companies. No standard scenario of digital image processing algorithms for crack detection is available and guarantees in all crack pavement images cases. Previously several image processing algorithms for crack detection are suffering from various shortcomings on crack detection sides. This work provides

proposed automated image processing crack detection algorithm. The goal is to automatically extract and classify the linear crack and its characteristics from sequence pavement images of different streets. The sequence pavement images (mobile mapping data) were observed by two Germany companies as follows : LEHMANN + PARTNER GmbH company using S.T.I.E.R mobile mapper system and 3D Mapping Solutions GmbH company using MoSES mobile road mapping system. In addition, two case studies were observed by Unicom-Umap company using VISAT™ mobile mapping system -Saudi Arabia.

The overall proposed algorithm is used for testing various pavement crack images from different countries. The performance is checked by comparing the results with well-known crack detection algorithms. Obviously, the validation process is deviated by 3.8 min (processing time) and 98.9% (percentage of correctness rate) for around 96 continuous mobile mapping images (Lehmann + Partner GmbH company images-Germany). 16.2 min in average and 100% for around 336 continuous mobile mapping images (3D-mapping Solution GmbH company images-Germany) could be achieved. Moreover, in average 15.6 min and 100% for around 200 continuous mobile mapping images (Unicom-Umap company images-Saudi Arabia) could be obtained. Figure 15 illustrates the final resultant images with network of cracks (block type) and vertical individual cracks and their characteristics.

Figure 15: Final resultant images with vertical individual cracks and network of cracks (block type) and their characteristics.

Geodetic Control of FEM-Model from plane load-bearing structures

The goal of this investigation is to verify the simulation model with the reality. The investigated plane load-bearing structure is the thin double curved structure Stuttgart SmartShell. Stuttgart SmartShell has a base area of about 100 m² and a thickness of 4 cm. It is made of multilayer wood. Stuttgart SmartShell is resting on four supports. One of these supports is static, while the other three are mobile. The main reason to develop a structure like Stuttgart SmartShell is to investigate possibilities for constructions which offer an active manipulation in order to reduce structural vibrations and stress. In the same time the weight of the structure is drastically reduced. Figure 16 shows Stuttgart SmartShell.

Figure 16: Stuttgart SmartShell (© Bosch Rexroth).

The mobile supports of Stuttgart SmartShell can be moved in the three directions X, Y and Z. During the investigation with the Laser Scanner Leica HDS 7000, all supports are moved sequential in all three directions. After each measurement the support is moved back to the initial position. The movement is 20 mm in each direction.

The FEM-Model and the scans are modelled as NURBS. The comparisons between the initial position and the different movements show results like expected through the comparison of the FEM-Models in the same position. More interesting is the comparison between the FEM-Model and the scans in each position, because the scans show the actual measured state and the simulation the model state. For this comparison the scans are transformed with a classical 3D-Helmert-Transformation to the coordinate system of the FEM-Model. The transformation parameters are determined once in the initial position and used for all other positions, too. Multiple statistical tests are made for all positions. Due to this test there are no significant deviations, but the results are not realistic, because there are deviations bigger than 33 mm. One reason for the non-significant deviations could be correlations between the measurements. The next steps should be the integration of influences due to weather, waterproofing and grinding into the FEM-Model. For further scans the scanner errors should be investigated in detail and considered in the tests.

Location Referencing

With the growing availability of powerful and cost-efficient mobile devices as well as area-wide mobile communication networks, more and more applications are being developed in the consumer and professional sector (e.g. the automotive industry) that assign a location, the so-called georeference, to the transmitted information. In a geodetic sense, a georeference consists of a set of coordinates in a defined coordinate system and marks a place on earth in a distinct way. For practical application, however, it is often helpful to add links to real-world objects, e.g. buildings or roads to these coordinates. A catalogue of such mappings of real-world objects together with their description in general can be regarded as a (digital) map. To be able to exchange information that is referenced on objects of such a map, a standardized generalization of the georeference is required. This is typically referred to as Location Referencing.

Location Referencing techniques have been developed, implemented and practically utilized within a number of research projects. Within the EU-funded research project ROSATTE, for example, it became apparent that these LR-techniques are suitable for the transmission of map-based information between different map systems. For certain applications with high quality requirements, however, further improvements of these existing LR-methods are required.

Location Referencing can basically be differentiated in static and dynamic Location Referencing. Typical LR applications show a high dynamic together with high requirements on up-to-dateness and the need of immediate adaption to real-world changes. For that reason, a static referencing with centrally administrated location tables seems to be less reasonable for current and future practical applications of Location Referencing. Since it is already widely used and accessible with respect to its license and implementation, OpenLR is used and analysed in detail as a basis for further developments. For that reason, the corresponding OpenLR Whitepaper as the published standard and the reference implementation that is publicly available from the OpenLR website are investigated in detail and possibilities of improvement identified.

Based on the preceding analysis, a new Location Referencing method, the so-called form-matcher, has been developed in a thesis. The new method builds up on OpenLR, but uses additional, form-based matching parameters, e.g. the number of significant direction changes of a linear location reference. For the search for possible matching candidates, the complete course of the route of the location reference is considered in the target network. Then these identified route candidates are individually investigated using the selected matching parameters. Furthermore, the new method considers the topological properties of the location references in particular for the decoding in the target network.

The quality specification of the map assignments and therewith also the evaluation of the LR transmissions should be based on existing quality models. Therefore, general approaches of quality specification of geodata in geoinformatics as well as the traffic and transportation domain, respectively, are investigated. Beyond that, existing approaches of quality description and modelling, for example the one derived from the ROSATTE research-project or the widely-used precision-recall approach are examined with respect to their suitability for the use.

Finally, the newly developed LR method together with the quality assessment methodology was implemented in the so-called LR testbed, to enable practical investigations. The empirical investigations that have been carried out using different datasets show a quality improvement of the form-matcher LR transmissions. For one direction (from map 1 to map 2) of transmission, the share of correct assignments could be raised from 63 % to 75 %. For the opposite direction, however, OpenLR shows a higher quality level with a portion of 71 % of correct assignments that could not be improved by the form-matcher with its 69 % correctness.

Ghosthunter - Telematics System against ghost drivers using GNSS

In cooperation with the University of the Armed Forces Munich (UniBwM) and the company NavCert in Braunschweig, a telematics system will be implemented to detect ghost drivers with the use of GNSS and digital road maps, which could help to improve highway and auto safety greatly. A ghost driver is an individual who travels in a wrong direction or completely against the flow of traffic. Such wrong-way driving is responsible for about 2,000 accidents and 20 fatalities on the German autobahn every year, which are usually due to drunken driving or maybe also a suicide attempt. The purpose of the project called „Ghosthunter" is to contribute to preventing and managing ghost driver incidents.
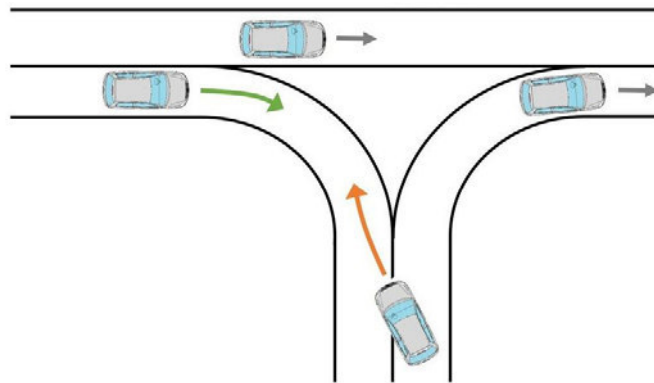

Figure 17: host driver on German autobahn (source: UniBwM).

How can we detect ghost driving at an early stage and reliably, shake the wrong-way driver up efficiently and warn endangered road users in the surrounding area? In the project „Ghosthunter" this problem will be solved with a selected research method based on GNSS and spatial road maps. With a robust (D)GNSS-based algorithm developed by UniBwM, accurate vehicle trajectories (movement path) will be recorded and used in the map-matching algorithm to locate the vehicle on the road. However, before developing practical map-matching algorithms, data qualities of digital road maps of four different map providers (ATKIS, Here, TomTom and OSM) should

be investigated with certain quality criteria. The absolute accuracy is evaluated by comparing every reference point (based on precise GNSS differential carrier-phase positioning) with its foot of perpendicular in the map line.

$$dx_i = x_{\text{gps},i} - x_{\text{lfp},i} \tag{5}$$

$$dy_i = y_{\text{gps},i} - y_{\text{lfp},i} \tag{6}$$

$$d_{x,y} = \sqrt{\sum_{i=1}^{n} dx_i^2 + dy_i^2} \tag{7}$$

For valuating relative accuracy, two criteria will be chosen: one criterion is the difference of orientation changes between every map point and its homologous point of reference data

$$\Delta\Delta\alpha = \Delta\alpha_{\text{gps}} - \Delta\alpha_{\text{map}} \tag{8}$$

and the other is the determination of the curvature difference between every map point and its homologous point of reference data.

$$\Delta K = K_{\text{gps}} - K_{\text{map}} \tag{9}$$

After reliable and comprehensive evaluations as well as consistency checks of ATKIS, Here, Tom-Tom and OSM, the results show that all these four maps have reached an accuracy level of 2 meters for absolute position and 1 meter for relative accuracy.

Publications

Refereed Publications

Abdallah, A., Schwieger, V.: Kinematic Precise Point Positioning (PPP) Solution for Hydrographic Applications. FIG Working Week 2015, Sofia, Bulgaria, 2015.

Laufer, R., Schwieger, V.: Modeling Data Quality Using Artificial Neural Networks. In: Kutterer, H., Seitz, F., Alkhatib, H., Schmidt, M.: The 1st International Workshop on the Quality of Geodetic Observation and Monitoring Systems. Heidelberg, Springer, 2015.

Lerke, O., Schwieger V.: Evaluierung der Regelgüte für tachymetrisch gesteuerte Fahrzeuge. In zfv - Zeitschrift für Geodäsie, Geoinformation und Landmanagement, Heft 4/2015 - 140. Jahrgang.

Schmitt, A., Schwieger, V.: Quality Control of Robotics Made Timber Plates. FIG Working Week 2015, Sofia, Bulgaria, 2015.

Schweitzer, J., Schwieger, V.: Modeling and Propagation of Quality Parameters in Engineering Geodesy Processes in Civil Engineering. In: Kutterer, H., Seitz, F., Alkhatib, H., Schmidt, M.: The 1st International Workshop on the Quality of Geodetic Observation and Monitoring Systems. Heidelberg, Springer, 2015.

Non-Refereed Publications

Abdallah, A.: The Effect of Convergence Time on the Static-PPP Solution. Proceedings on 2nd International workshop on „Integration of Point- and Area-wise Geodetic Monitoring for Structures and Natural Objects", March 23-24, 2015, Stuttgart, Germany.

Abdallah, A., Schwieger, V.: PPP for Hydrography. GPS World Magazine, 26 (12), pp 52-55.

Al-Mistarehi, B., Schwieger, V.: Automated Detection for Pavement Crack for Mobile Mapping Data. Proceedings on 2nd International workshop on „Integration of Point- and Area-wise Geodetic Monitoring for Structures and Natural Objects", March 23-24, 2015, Stuttgart, Germany.

Breitenfeld, M.; Wirth, H.; Brüggemann, T.; Scheider, A.; Schwieger, V. (2015): Entwicklung von Echtzeit- und Postprocessingverfahren zur Verbesserung der bisherigen Ortung mit Global Navigation Satellite Systems (GNSS) durch Kombination mit weiteren Sensoren sowie hydrologischen Daten. (Projektabschlussbericht HydrOs).

Karpik, A., Schwieger, V., Novitskaya, A., Lerke, O. (Hrsg.): Proceedings on 2nd International workshop on „Integration of Point- and Area-wise Geodetic Monitoring for Structures and Natural Objects", March 23-24, 2015, Stuttgart, Germany.

Kauker,S., Schwieger, V.: Approach for a Synthetic Covariance Matrix for Terrestrial Laser Scanner. Proceedings on 2nd International workshop on „Integration of Point- and Area-wise Geodetic Monitoring for Structures and Natural Objects", March 23-24, 2015, Stuttgart, Germany.

Schmitt, A.: Deformation Analysis of a Timber Pavilion. Proceedings on 2nd International workshop on „Integration of Point- and Area-wise Geodetic Monitoring for Structures and Natural Objects", March 23-24, 2015, Stuttgart, Germany.

Schwieger, V., Beetz, A.: Baumaschinensteuerung aus ingenieurgeodätischer Sicht. 145. DVW-Seminar: Interdisziplinäre Messaufgaben im Bauwesen - Darmstadt 2015, 26.-27.03.2015.

Schwieger, V., Schmitt, A.: Quality Control and Deformation Analysis for a Timber Construction. GeoSiberia 2015, Novosibirsk, Russia, 20.-22.04.2015.

Wirth, H., Breitenfeld, M., Scheider, A., Schwieger, V.: HydrOs - Ein integriertes Ortungssystem kombiniert mit hydrologischen Daten. Hydrographiosche Nachrichten, Heft 6, 2015.

Zhang, L.: Reducing Multipath Effects by Considering Spatial Correlation. Proceedings on 2nd International workshop on „Integration of Point- and Area-wise Geodetic Monitoring for Structures and Natural Objects", March 23-24, 2015, Stuttgart, Germany.

Zhang, Lif., Zheng, B.: Denoising of the Point Cloud for Deformation Analysis. Proceedings on 2nd International workshop on „Integration of Point- and Area-wise Geodetic Monitoring for Structures and Natural Objects", March 23-24, 2015, Stuttgart, Germany.

Zhang, W., Zhang, L.: Time Series Analysis of Different Shieldings of Low-Cost GPS Receiver. Proceedings on 2nd International workshop on „Integration of Point- and Area-wise Geodetic Monitoring for Structures and Natural Objects", March 23-24, 2015, Stuttgart, Germany.

Presentations

Scheider, A.: „Erweiterung eines Multi-Sensorsystems zur Positionsbestimmung von Vermessungsschiffen", PhD-Seminar, DGK Section Engineering Geodesy, 7./8. May 2015, Stuttgart.

Activities at University and in National and International Organisations

Volker Schwieger
Vice Dean of Faculty of Aerospace Engineering and Geodesy, University of Stuttgart
Spokesperson of Centre for Transportation Research at University of Stuttgart (FOVUS)
Executive Board of Cooperation German Rail (DB) and University of Stuttgart
Chair of FIG Commission 5 „Positioning and Measurement"
Head of Working Group III „Measurement Methods and Systems" of Deutscher Verein für Vermessungswesen (DVW)
Chief Editor of Peer Review Process for FIG Working Weeks
Member of Editorial Board Journal of Applied Geodesy
Member of Editorial Board Journal of Applied Engineering Science
Member of Editorial Board Journal of Geodesy and Geoinformation

Martin Metzner
Member of the NA 005-03-01 AA „Geodäsie" at the DIN German Institute for Standardization

Li Zhang
Vicechair of Administration of FIG Commission 5 „Positioning and Measurement"
Member of Working Group III „Measurement Methods and Systems" of Deutscher Verein für Vermessungswesen (DVW)

Diploma Theses and Master Theses

Bosch, Jascha: Evaluierung der Regelgüte beim Einsatz von GNSS Sensoren im Baumaschinen-simulator (Supervisor: O. Lerke)

Fedan, Mehdi: Design and development of a laser-scanning system for documentation of objects of cultural heritage (Supervisor: M. Metzner)

Haji Sheikhi, Meysam: Accuracy Analysis for the Low-Cost GPS Antennas with different Shield-ings (Supervisor: L. Zhang)

Huang, Xingyun: Check the stability and independence of buildings movement for the measure-ment pillars in the measuring cellar (Supervisor: A. Hassan)

Kizilirmak, Gökhan: Detection and Reconstruction of the Catenary of a Rail Track Using Laser Scanning (Supervisor: M. Metzner)

Laatsch, Stephan: Vernetzung zweier Tachymeter zur automatischen Zielverfolgung (Supervisors: A. Scheider, O. Lerke)

Lafte, Meisam Alhajaj: Sensitivity Analysis and Design of Monitoring Networks Purposing Predic-tion of Landslides (Supervisor: O. Lerke)

Nanic, Milos: Development of the Vehicle and Motion Model for Construction Machines for a Kalman Filter (Supervisor: O. Lerke)

Obaid, Jehad: Map-Matching Algorithm: State of the Art and New Developments Concerning Real-Time Procedures and Open Street Map (Supervisor: M. Metzner)

Pitzer, Philipp: Ansatz zur Kartierung von Autobahnen für das autonome Fahren durch Mehrfach-befahrungen mittels potentieller Sensorik zukünftiger Serienfahrzeuge (Supervisor: M. Metzner)

Poptean, Sabina: Applications of terrestrial laser scanning and laser tracker for deformation anal-yses of a supporting structure (Supervisor: A. Schmitt)

Reuter, Philipp: Entwicklung eines Fuzzy-Reglers zur hochgenauen, autonomen Steuerung eines Baumaschinensimulators (Supervisor: O. Lerke)

Scatturin, Raphael: Entwicklung eines Kalman Filters für die Fusion von GPS- und Beschleuni-gungsdaten (Supervisors: A. Scheider, M. Metzner)

Schaal, Carolin: Deformationsuntersuchung am Rutschhang Hessigheim (Supervisor: A. Hassan)

Taschke, Simon: Contributions to the GNSS Positioning using virtual RINEX observation files. (Supervisor: L. Zhang)

Wang, Yuqi: Optimization of the Transient Oscillation during the Control of a Vehicle on a Given Trajectory (Supervisor: O. Lerke)

Ye, Zican: Untersuchung von TMC Nachrichten zum Nutzen in ADAS sowie Optimierung eines TMC-Generators (Supervisor: M. Metzner)

Study Theses and Bachelor Theses

Aichinger, Julia: Grundlagen und Beispielrechnungen zu NURBS (Supervisor: A. Schmitt)

Föll, Andreas: Untersuchung der Reflexivität unterschiedlicher Materialien (Investigations on the reflctivity of different materials) (Supervisor: S. Kauker)

Fischer, Jonas: Untersuchungen zur Kalibrierung des Laserstrackers API Radian. (Supervisor: A. Schmitt)

Graner, Martin: Echtzeit-Positionsbestimmung mittels bewegter Tachymeter (Supervisor: A. Scheider)

Kappler, Marius: Evaluierung eines Tachymeters als bewegter Sensor in einem Positionierungssystem (Supervisor: A. Scheider)

Reuter, Philipp: Weiterentwicklung des Mobilen Positionierungssystems MOPSY (Supervisor: O. Lerke, M. Metzner)

Wenzl, Florian: Rekonstruktion der Portaloberfläche vom Münster zum Heiligen Kreuz für die Deformationsanalyse (Supervisor: B. Zheng, V. Schwieger)

Education

SS15 and WS15/16 with Lecture/Exercise/Practical Work/Seminar

Bachelor Geodesy and Geoinformatics

Basic Geodetic Field Work (Schmitt, Kanzler)	0/0/5 days/0
Engineering Geodesy in Construction Processes (Schwieger, Kauker)	3/1/0/0
Geodetic Measurement Techniques I (Metzner, Schmitt)	3/1/0/0
Geodetic Measurement Techniques II (Schmitt)	0/1/0/0
Integrated Field Work (Metzner, Kauker)	0/0/10 days/0
Reorganisation of Rural Regions (Helfert)	1/0/0/0
Statistics and Error Theory (Schwieger, Zhang, Wang)	2/2/0/0

Master Geodesy and Geoinformatics

Deformations Analysis (Schwieger, Zhang)	1/1/0/0
Industrial Metrology (Schwieger, Kanzler, Schmitt)	1/1/0/0
Land Development (Eisenmann)	1/0/0/0
Monitoring Project (Lerke)	0/0/2/0
Monitoring Measurements (Schwieger, Wang)	1/1/0/0
Causes of Construction Deformation (Metzner/Scheider/Wang)	1/1/0/0
Transport Telematics (German) (Metzner, Scheider)	2/2/0/0
Thematic Cartography (German) (Metzner)	1/1/0/0
Terrestrial Multisensor Data Acquisition (German) (Zheng, Lerke)	1/1/0/0

Master GeoEngine

Integrated Field Work (Metzner, Kauker)	0/0/10 days/0
Kinematic Measurement Systems (Schwieger, Lerke)	2/2/0/0
Monitoring (Schwieger, Wang)	1/1/0/0
Thematic Cartography (Metzner, Kauker)	1/1/0/0
Transport Telematics (Metzner, Hassan)	2/1/0/0

Bachelor and Master Aerospace Engineering

Statistics for Aerospace Engineers (Schwieger, Zhang, Hassan)	1/1/0/0

Master Aerospace Engineering

Transport Telematics (German) (Metzner, Scheider)	2/2/0/0

Bachelor Civil Engineering

Geodesy in Civil Engineering (Metzner, Scheider)	2/2/0/0

Master Civil Engineering

Geoinformation Systems (Metzner, Hassan)	2/1/0/0
Transport Telematics (Metzner, Scheider)	1/1/0/0

Bachelor Technique and Economy of Real Estate

Acquisition and Management of Planning Data and Statistic (Metzner, Kanzler)	2/2/0/0

Bachelor Transport Engineering

Statistics (Metzner, Kanzler)	0.5/0.5/0/0
Seminar Introduction in Transport Engineering (Hassan)	0/0/0/1

Master Infrastructure Planning

GIS-based Data Acquisition (Zhang, Schmitt)	1/1/0/0

Institute of Geodesy

Geschwister-Scholl-Str. 24D, D-70174 Stuttgart,
Tel.: +49 711 685 83390, Fax: +49 711 685 83285
gis@gis.uni-stuttgart.de or firstname.secondname@gis.uni-stuttgart.de
http://www.gis.uni-stuttgart.de

Head of Institute

Prof. Dr.-Ing. Nico Sneeuw

Emeritus

em. Prof. Dr.-Ing. habil. Dr.tech.h.c.mult. Dr.-Ing.E.h.mult. Erik W. Grafarend

Academic Staff

Dr.-Ing. Markus Antoni	Physical Geodesy, Satellite Geodesy
Prof. Dr. sc. techn. Wolfgang Keller	Physical Geodesy, GNSS
Dr.-Ing. Friedrich Krumm	Adjustment Theory, Mathematical Geodesy
Dipl.-Ing. Matthias Roth	Physical Geodesy, Satellite Geodesy
Dr.-Ing. Mohammad Tourian	Satellite Geodesy, Hydrology

Research Associates

M.Sc. Qiang Chen (until 27.11)	Satellite Geodesy
M.Sc. Omid Elmi	Remote Sensing
Dr.-Ing. Siavash Iran Pour	Future Satellite Missions
M.Sc. Muhammad A. Javaid	Satellite Geodesy
M.Sc. Huishu Li (until 28.08)	Satellite Geodesy
M.Sc. Wei Liu	Satellite Geodesy
M.Sc. Shirzad Roohi	Altimetry, Hydrology
M. Tech. Bramha Dutt Vishwakarma	Hydrology, Filter Methods
M.Sc. Jinwei Zhang	Satellite Geodesy, Hydrology

Administrative/Technical Staff

Dipl.-Ing. (FH) Thomas Götz	IT System, Controlling
Dipl.-Betriebsw. (FH) Wanda Herzog	Study Course Management
Dipl.-Ing. (FH) Ron Schlesinger	IT System, Technical Support
Anita Vollmer	Secretary

Guests

Dr. M Scheinert, TU Dresden (02.02.-24.02.)
Prof. Dr.-Ing. RJ You, National Cheng Kung University, Tainan, Taiwan (02.03.- 28.05)
Prof. A Borkowski, Wrozlaw/Poland (20.4.-24.04.)
Assoc. Prof. Y Lin, Tongji/China (18.09.14-31.12.15)
Prof. Dr. E Issawy, Cairo/Egypt (26.6.-9.7.)
Prof. Dr. M Sharifi, Tehran/Iran (14.-18.9.)
Prof. Dr. H Wen, CASM Beijing/China (1.11.-31.12.)
Prof. Dr. W Jiang, Vice Dean SGG, Wuhan University, China (1.11.-31.12.)
Prof. Dr. Y Yao, Dean SGG, Wuhan University/China (8.12.-31.12.)
Prof. Dr. W Shen, Wuhan University, China (1.11.-31.12.)
Dr. B Ke, CASM Beijing, China, from 24.11.

External Lecturers

Dipl.-Ing. Steffen Bolenz, Stadtmessungsamt, Stuttgart
PD Dr.-Ing. habil. Johannes Engels, Stuttgart
Dipl.-Ing. Dieter Heß, Ministerium für Ländlichen Raum und Verbraucherschutz
  Baden-Württemberg, Stuttgart
Dipl.-Ing. Günther Steudle, Ministerium für Ländlichen Raum und Verbraucherschutz
  Baden-Württemberg, Stuttgart

Research

Pre-Mission Error Assessment for the Pendulum Formation

Semi-analytical approach

The design of future gravity field missions requires the prediction of the formal error due to orbit constellation and the instruments. One tool for that purpose is the *semi-analytical approach*, which is based on re-writing the observable $f^{\#}$ (potential differences, range, range-rate, orbit radius...) in a 2D Fourier series, where the (lumped) Fourier coefficients $\underline{\mathbf{A}}_{mk}^{\#}$ are a linear combination of the Stokes coefficients $\bar{K}_{lm}$ and the transfer matrix $\underline{\mathbf{H}}_{lmk}^{\#}$ of the observable. The formal errors σ_{lm} of the gravity field coefficients are then determined by error propagation, i.e. the diagonal of the matrix $\left((\underline{\mathbf{H}}_{lmk}^{\#})^{\top} \underline{\mathbf{P}} \, \underline{\mathbf{H}}_{lmk}^{\#} \right)^{-1}$.

On the one hand, the method requires

 ▷ constant nominal orbit parameters (height, inclination,...),

 ▷ a stochastic model of the instruments for the weight matrix $\underline{\mathbf{P}}$

 ▷ and the observation type,

but neither (simulated) data nor orbit integration (Figure 1). In addition, the matrix inversions can be performed for each order m separately, which leads to a very effective error assessment.

On the other hand, the method is restricted to

 ▷ constant gravity field without tides or mass changes

 ▷ and constant orbital parameters.
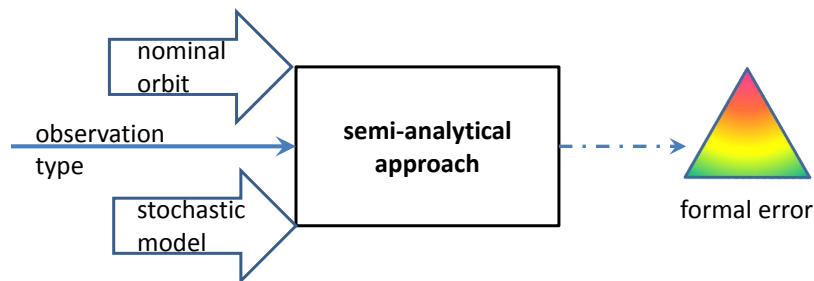
Figure 1: Concept of the semi-analytical approach
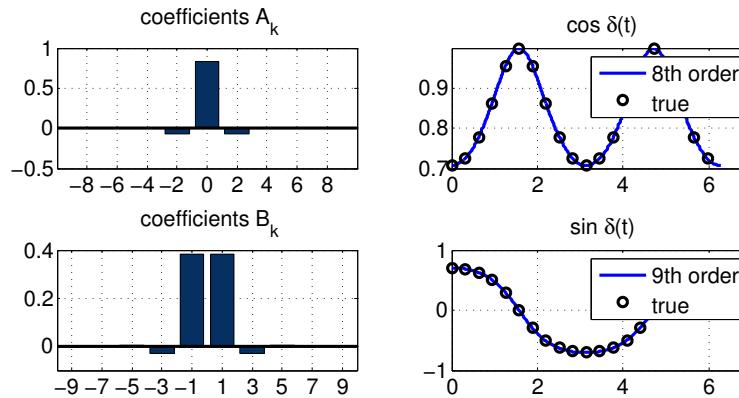
Figure 3: Approximation of $\sin\delta(t)$ and $\cos\delta(t)$ terms by Fourier series

Pendulum constellation

The pendulum constellation consists of 2 satellites with the same orbital height and inclination, but a different nodal line/orbital plane. Between the satellites, a ranging system (microwave or laser) is installed to measure the (relative) range, range-rates or range-accelerations (Figure 2).

The observation contains a time-variable combination of along-track and cross-track components, which leads to a improvement for gravity field coefficients compared to GRACE-mission-like missions. The opening angle $\delta(t)$ between flight direction and the second satellite is periodically changing (cf. Figure 3), with a maximum value δ_0 at the equator. This variation contradicts the previous restriction of a constant orbit geometry in the semi-analytical approach.

The problem is solved by expressing the temporal variations (here: sine and cosine of opening angle $\delta(t)$ and central angle $\eta(t)$) in Fourier series and insert into the transfer matrix $\underline{\mathbf{H}}^{\#}_{lmk}$. After re-indexing and exchanging the order of summation, the entries can be interpreted as a *convolution*. The additional Fourier series converges rapidly, so that the increase of numerical effort and matrix dimensions is limited (cf. Figure 3).
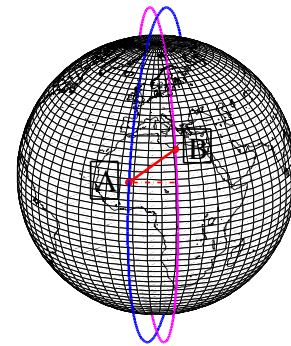
Figure 2: Pendulum constellation

Simulation

In a first simulation, two polar satellites are chosen in the height of $h = 335$ km, which leads to a repeat orbit after 32 nodal days. White noise with $10^{-8} \frac{m}{s}$ is assumed for the range-rate and an average distance of $\rho_{avg} = 75$ km. The formal errors are arranged in the triangular spectrum and presented for different opening angles δ_0 in Figure 4.
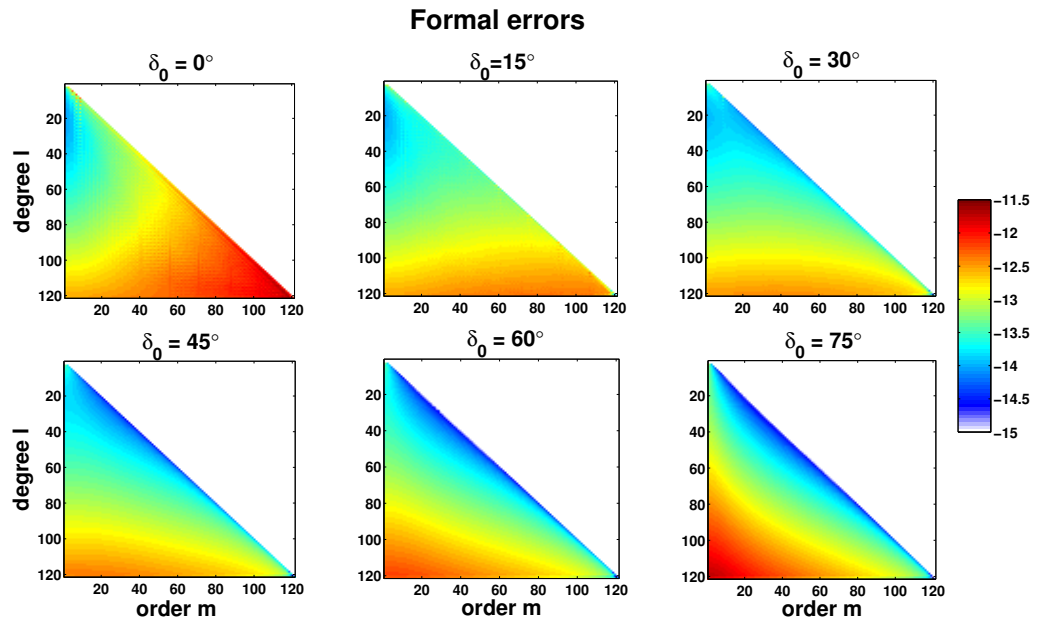
Figure 4: Formal error for pendulum constellations with different opening angles and white noise

Apart form the magnitude of the formal errors, also their homogeneity is subject of investigation. In case of homogeneous formal errors, the quality of the estimated field is independent of the direction, and so the GRACE-like stripes would vanish. Homogeneity is visible in the triangular spectrum by constant colors per line. The most homogeneous error spectrum is found for an opening angle $\delta_0 = 30°$ in upper right picture. For GRACE-like missions with $\delta = 0°$, the 'near-zonal' coefficients $m \approx 0$ are better determined, while for larger opening angles, the 'near-sectorials' have lower formal errors.

Impact of Groundtrack Pattern of Double Pair Missions on the Gravity Recovery Quality

The launch of the GRACE mission brought a broad interest within the geophysical community in monitoring temporal gravity field. Due to the limited lifetime of GRACE, several studies have been conducted for the search of optimal GRACE follow-on and future satellite gravity missions . These studies mainly discuss the use of alternative formations like Pendulum, Cartwheel and LISA as well as the double inline pair missions with different orbits as a possible substitute of the current GRACE mission. The double satellite pair configuration in a so-called Bender constellation, however, is currently in the focus of research into time-variable gravity field recovery by future satellite missions, where the primary objective is to achieve higher temporal and spatial resolutions.

When looking for optimal double inline missions, one important subject is the impact of the ground-track pattern of such missions on the quality of gravity recovery. The investigation of pattern distribution impact on the recovery quality may lead to better understanding of orbital parameters to be optimized. This study, in particular, investigates the influence of longitude of the ascending node difference of two pairs in a double pair mission. The research aims to show how the variations in ascending node difference change the quality of gravity solutions to the large extent. The impact of the time-variable gravity field itself on the error level of the gravity solutions is also shown.

Drifting orbits of satellite pairs

As we expect, the ground-track pattern distribution of double pair mission changes within the time. Obviously, the main reason for this variation is the different gap evolution of the repeat orbits of the two pairs. One important factor for the ground-track pattern variation is simply the change of the difference of the longitude of the ascending nodes between the satellite pairs ($\Delta\Omega$) as well as the mean anomaly between the pairs (ΔM), where the parameters Ω and M of each satellite pair change within the time, as follows:

$$\dot{\Omega} = \frac{1}{na^2\sqrt{1-e^2}\sin I}\frac{\partial T}{\partial I} \tag{1a}$$

$$\dot{M} = n - \frac{1-e^2}{na^2 e}\frac{\partial T}{\partial e} - \frac{2}{na}\frac{\partial T}{\partial a} \tag{1b}$$

with a, e and I for respectively the semi-major axis, eccentricity (here sets to zero for the circular orbits) and inclination angle, $n = \sqrt{\frac{GM}{a^3}}$ as the mean motion of the satellite and T as the disturbing potential field.

Therefore, from the relative variations of the parameters Ω and M of the two pairs, the time evolution of ground-track pattern of the dual pair mission scenarios is expected to be more complicated than the single pair cases.

Table 1: A selected double pair mission scenario.

scenario	β/α [rev./day]	inclination [deg.]	altitude [km]	sub-cycle [day]	ρ [km]
double pair	$172/11$	92	361.9	3	100
	$460/29$	115	342.5	7	

Impact of the groundtrack pattern variations on quality of the gravity solutions

In order to see the impact of $\Delta\Omega$ and ΔM on the recovery quality, we analyse the solutions of a selected double pair mission scenario (constellation scenario of Table 1) where only the relative Keplerian parameters $\Delta\Omega$ and ΔM change. Here, the gravity recovery of the scenario is simulated by "Reduced-Scale Tool" (RST) in which the satellites are orbiting the Earth in nominal orbits (only influenced by J_2 effect). We make use of "hydrology + ice + solid Earth" (HIS) geophysical signals as well as AO-error and ocean tide model error for the forwarding models of our simulation tool.

The pure impact of ground-track pattern evolution on the gravity recovery quality can be seen from Figure 5(a). The figure illustrates the recovery error of HIS signals in terms of geoid height RMS of one year time-series of 10-day solutions of the aforementioned scenario in which the HIS input signals within every 10 days are intentionally taken constant (i.e. no variation for the 10-day input signals within one year). That means only the ground-track pattern of every 10-day solution is different from the other solutions, and not the input signals themselves. However, as it is seen in the figure, we have still a spread of error curves (the red band) which means that the quality of the solutions varies by the pure effect of the ground-track pattern evolution.

Impact of gravity field variations on quality of the gravity solutions

It would be of our interest to also investigate the pure effect of time-variable gravity field when the ground-track pattern does not change within the gravity solutions. For this reason, we run our RST with changing gravity field of the HIS signals where within each 10-day solution, the Keplerian parameters for our nominal orbit simulation tool remain the same. The pure influence of time-variable gravity field is then illustrated in the Figure 5(b) where an error curves spread (red band) in terms of geoid height RMS is still observed. That means by keeping the groundtrack fixed, we still have variations in quality of gravity recovery.

Discussion

This research presented the impact of groundtrack pattern evolution and time-variable gravity field on the quality or error level of the gravity solutions. In case of the groundtrack impact, it is expected that the evolution of spatial-temporal sampling affects the quality of the gravity products. The sampling pattern of each satellite pair of a double pair mission with different repeat periods evolves
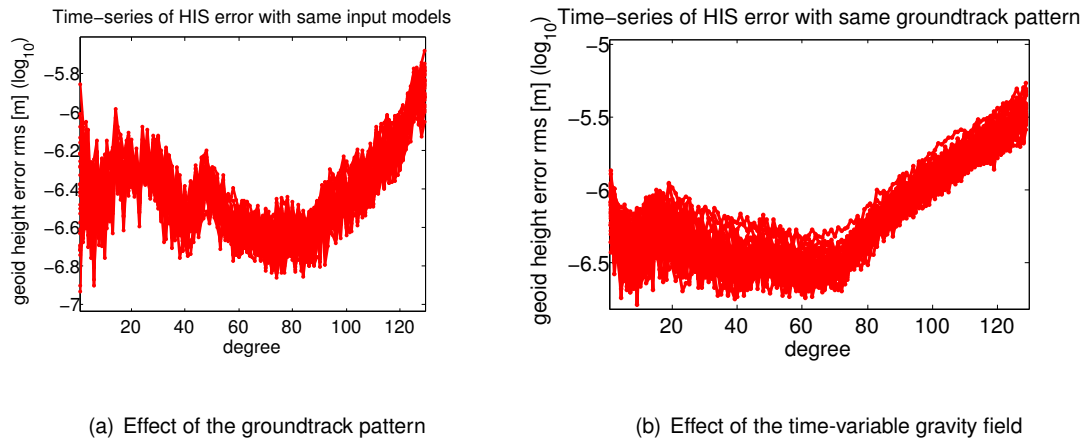
(a) Effect of the groundtrack pattern　　　　　　　(b) Effect of the time-variable gravity field

Figure 5: Recovery error spread of 1-year time-series of 10-day solutions of the Table 1 scenarios

differently in time domain. Therefore, one should expect that within a specific time-interval gravity solution, e.g. 10-day solution, the groundtrack pattern changes. Another reason for this variation is that the difference of the longitude of ascending nodes of the two pairs $(\Delta\Omega)$ changes within the time. That means the two orbits have different drifting rates, and hence different sampling pattern within each time window is expected. This fact makes the task of orbital parameters optimization challenging. In particular, that is the case for some of the optimal orbit search strategies such as genetic algorithm where we usually do the optimization for a single gravity solution and do not consider the time evolution of the solutions (time-series of gravity products) in our optimization procedure. On the other hand, this fact that the orbits of the single satellite pairs of a double pair mission have different drifting rates, opens new possibilities for orbit design in which one looks for specific spatial shift of the groundtrack pattern within the time intervals. In this case, by tuning the orbital parameters such as inclination angle of the satellite pairs and thus the orbital drifts, a desirable spatial sampling pattern shift can be achieved. Obviously for the future works and deeper insight into the subject, further investigations should be addressed in this way.
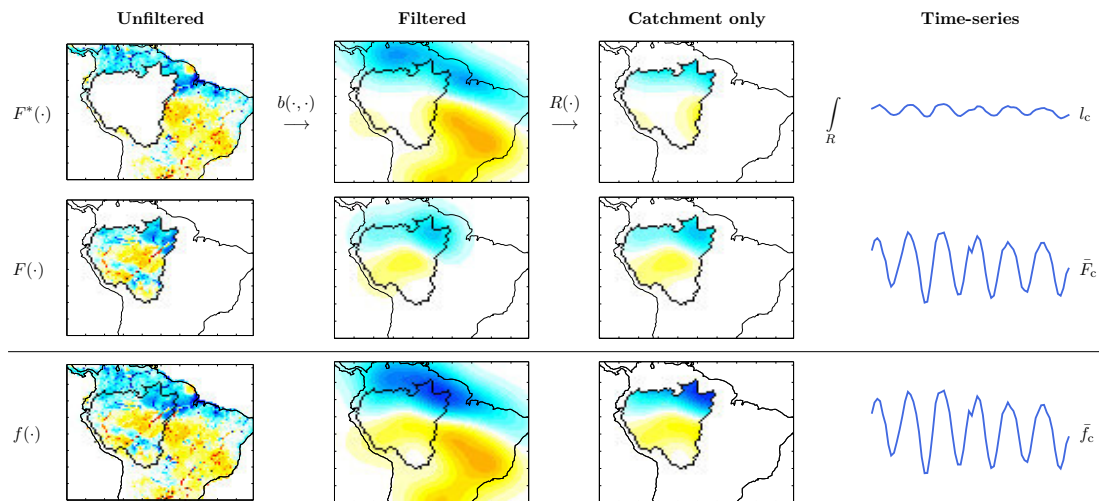
Figure 6: The first and the second rows are spatial complements of each other. The first row shows the leakage, and second row shows the signal loss, which is also termed as attenuation. The third row is the sum of the first two rows. Column 1 is filtered to obtain column 2. The field in column 2 is global, thus we extract the field only inside the catchment in column 3. Then the catchment average at each epoch of the field in column 3 constitutes a time-series, shown in column 4.

Catchment Scale Signal Changes due to Filtering

GRACE satellites have been observing the time-variable mass changes near the Earth surface since 2002. It is a valuable sensor to observe the temporal changes in underground water, the melting of glaciers and ice caps, and high magnitude Earthquakes. The products from GRACE satellites are contaminated with noise. Thus filtering is necessary to extract meaningful information. Filtering suppresses noise, but also changes the signal. The change in the signal at catchment scale can be understood by dividing it in two parts. Attenuation of the catchment aggregate due to spatial averaging, and leakage from outside due to convolution. To understand this visually please refer to the Figure 6.

The true catchment aggregate f_{c} is related to the catchment aggregate from filtered fields $\bar{f}_{\mathrm{c}}$.

Let l_{c} be the leakage and s be the scale factor to counter attenuation, then

$$\bar{f}_{\mathrm{c}} = \frac{1}{s} f_{\mathrm{c}} + l_{\mathrm{c}} \iff f_{\mathrm{c}} = s\left(\bar{f}_{\mathrm{c}} - l_{\mathrm{c}}\right). \tag{2}$$

$$s = \frac{f_{\mathrm{c}}}{\bar{F}_{\mathrm{c}}} = \frac{\int\limits_{\Omega} R(\theta, \lambda)\; \mathrm{d}\Omega}{\int\limits_{\Omega} R(\theta, \lambda)\, \bar{R}(\theta, \lambda)}\; \mathrm{d}\Omega \,. \tag{3}$$

In formula (3) s is a data independent catchment specific quantity for a given filter. $R(\theta, \lambda)$ is the catchment characteristic function (1 inside the catchment and 0 outside) and $\bar{R}(\theta, \lambda)$ is the filtered catchment characteristic function. $F(\theta, \lambda)$ is a field distribution multiplied by the catchment characteristic function, thus it has values only inside the catchment and outside the catchment it is zero. $\bar{F}_{\mathrm{c}}$ is the catchment aggregate of the filtered version of the field $F(\theta, \lambda)$. As per (2), first we should subtract l_{c} from $\bar{f}_{\mathrm{c}}$ and then scale up to reach f_{c}. This reduces the uncertainty in the catchment aggregates from filtered GRACE. We can compute the true catchment average, if we have accurate leakage information. So far we have discussed only the noise-free case, since GRACE fields are very noisy, the leakage computed is also noisy. A strategy is needed to determine l_{c}, which is our future work.

Basin Scale Runoff Prediction: an Ensemble Kalman Filter Framework based on Global Hydrometeorological Datasets

The importance of long-term monitoring of hydrological variables was recognized by the World Meteorological Organization (WMO) already in 1980, which led to the initiation of the Global Runoff Data Centre (GRDC). The GRDC collects and harmonizes global runoff observations from national hydrological services and makes them available to the public. However, over many catchments around the world, runoff is not gauged.

In a joint study with Karlsruhe Institute of Technology (KIT), Institute of Meteorology and Climate Research-Atmospheric Environmental Research, a data assimilation framework was proposed, which can be used to predict and correct basin-scale time-series of runoff. In general, the term data assimilation is used for combining observation data with hydrological, hydrometeorological, or land-surface models. The application usually ranges from extensive global reanalysis models, which simulate the whole atmosphere and the land surface, to models which focus on the land surface only. In this study the assimilation is based on the terrestrial water budget

$$P - ET - R - \dot{M} = 0 \;\;, \tag{4}$$

with precipitation P, evapotranspiration ET, runoff R, and water storage changes $\dot{M}$ appears simple, it is known from many studies that a real closure on larger spatial scales can not be achieved with current data sources.

One of the major design parameters of this study's framework is the use of as much real data as possible instead of using complex model equations. Thus, the approach is based on the terrestrial water budget equation, which is included in an Ensemble Kalman Filtering framework. The prediction scheme predicts precipitation, evapotranspiration, runoff, and water storage changes using
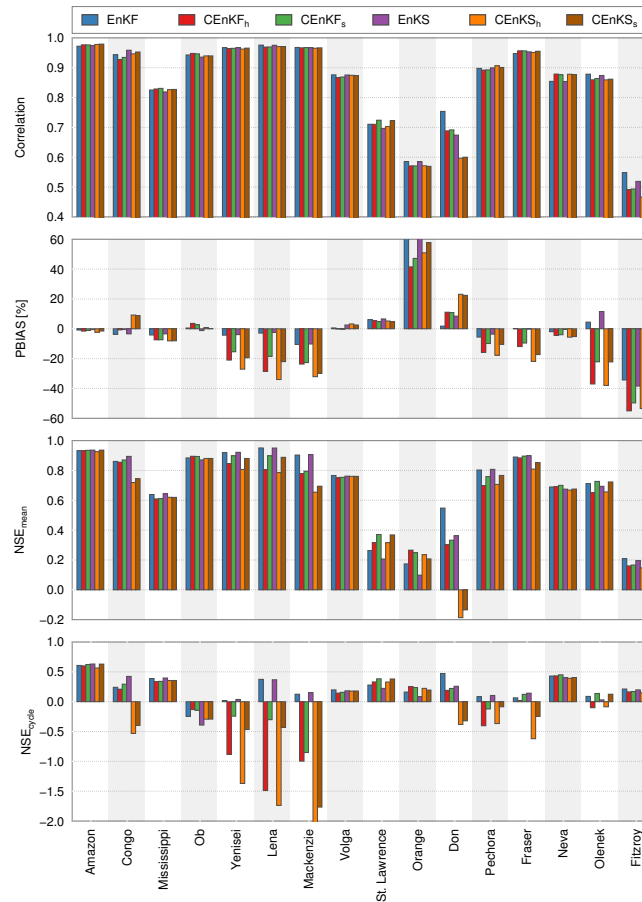
Figure 7: Performance metrics between observed and predicted runoff over all 16 study regions. The statistics are based on the period between 2005 and 2010. The colors indicate different configurations of the assimilation framework.

the so called least-squares prediction method. By this, we can exploit temporal and spatial co-variance structures between different catchments and water cycle variables. For the observation equations of the dynamic process model, the most recent versions of widely used data-sources for precipitation, evapotranspiration, runoff, and water storage changes are applied. We further use estimated runoff from satellite altimetry in order to both fill the gaps in the time-series of gauge-based runoff observations but also to improve the predictions.
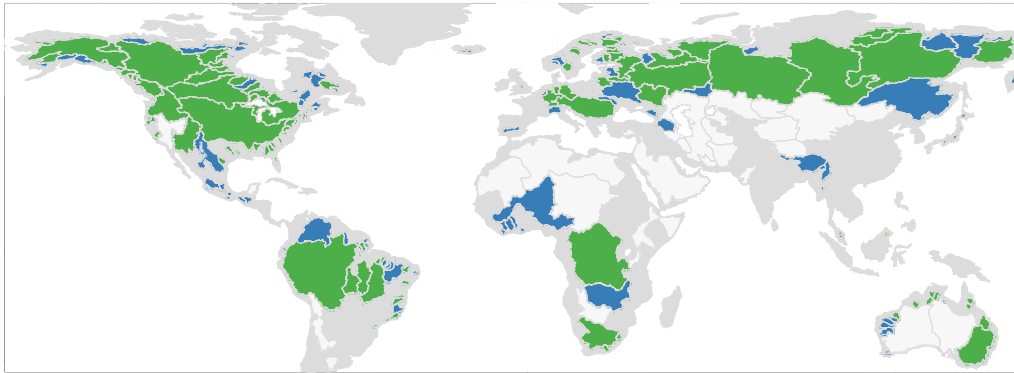
Figure 8: River basins for which runoff can be predicted using the Ensemble Kalman Filter approach based on global hydrometeorological datasets. For the green areas, more than 5 years of data after 2002 are available. The blue areas are (currently) poorly gauged basins with less than 5 years of data after 2002, but more than 5 years of continuous runoff measurements during the period 1980 to 2002. These catchments cover an area of more than $11\,500\,000\,\text{km}^2$ and provide a mean annual discharge volume of more than $125\,000\,\text{m}^3\!/\text{s}$ of freshwater resources.

In order to enforce water budget closure between the estimated parameters, further appropriate water budget constraints were added to the framework. Therefore, it is distinguished between hard constraints, which assume perfect closure of the water budgets, and soft constraints, which allow a small well defined imbalance. In the end, the framework is run in six different configurations: the Ensemble Kalman Filter (EnKF), the hard and soft Constrained Ensemble Kalman Filter (CEnKF_h, CEnKF_s), the Ensemble Kalman Smoother (EnKS), and the hard and soft Constrained Ensemble Kalman Smoother (CEnKS_h, CEnKS_s). In order to assess the performance of our data-assimilation approach, runoff is predicted over 16 large river basins and validated against *in situ* data. The performance analysis shows that the proposed method is able to estimate runoff with correlations larger than 0.8 for 12 of the 16 study regions 7. In terms of the PBIAS (representative of bias), values are less than $\pm 20\,\%$ for most of the catchments (except for Orange and Fitzroy). The NSE_mean-values (Nash-Suttcliffe efficiency coefficient with respect to long-term mean) are larger than 0.5 for 13 of the 16 catchments. As the runoff time-series of several catchments are dominated by a strong annual cycle, we further analyze the NSE_cycle (Nash-Suttcliffe efficiency coefficient with respect to average annual cycle), which relates the performance of the predictions to the long-term mean annual cycle. For 15 of the 16 study basins, at least several configurations achieve NSE_cycle-values larger than 0. The time-series clearly show that the reason for this good performance is a promising agreement between the observed and predicted long-term variations in the runoff time-series.

As a conclusion, the method is able to provide runoff estimates over the catchments shown in Figure 8, where only few or even no runoff observations are available after the year 2002. These catchments cover an area of more than $11\,500\,000\,\text{km}^2$ and provide a discharge volume of more than $125\,000\,\text{m}^3\text{/s}$ of freshwater resources.

The performance analysis emphasizes the promising performance of the proposed method for predicting runoff. To the best of our knowledge, such results (especially on a global scale) have never been reported by any study so far.

River Discharge Estimation Using Channel Width from Satellite Imagery

River discharge has been measured for more than a century directly near the river section. Despite various attempts, some basins are still unmonitored. Moreover, since 1970s the number of worldwide gauging stations have decreased from near 8000 to less than 2000 since 1970s which lead to 75% reduction in annual stream flow monitoring. This situation increases the interest to apply remote sensing data for hydrological purposes while they are able to observe and monitor different physical parameters of river which can be a representative of discharge. In a natural river section, behaviour of different physical parameters of river like discharge, water level and river width are strongly correlated to each other. It means that by measuring a parameter like river width we can estimate the river discharge via an empirical function developed based on simultaneous observations from two dataset.

To develop an empirical function between river width and discharge, a sufficient number of satellite images must be acquired simultaneously with in situ data. When the relationship is established, river discharge could be estimated without in situ observation. This could be serious restriction in river discharge monitoring as less than 50% of gauging stations have not been functioned after 2000. Moreover, a large historical data set of in situ discharge measurements remains useless, for which no coincidence spaceborne measurements are available. To overcome this obstacle, we find a relationship between river width and river discharge based on quantile function mapping with data sets acquired in different time frame.

We follow classical hydraulic relationship in a natural river cross section assumed a power law relationship between river discharge and width

$$Q = aW^b,$$

where river discharge Q is defined as a product of river section width W, a and b are the coefficients to be estimated via a weighted total least square (WTLS). By applying this technique we are able to estimate discharge together with its uncertainty. Details about case study is provided in Figure 9 and Table 2.

Simultaneous observations approach

All the simultaneous measurements from two datasets during the training period are plotted in a two dimensionals scatterplot and then unknown regression coefficients are estimated.
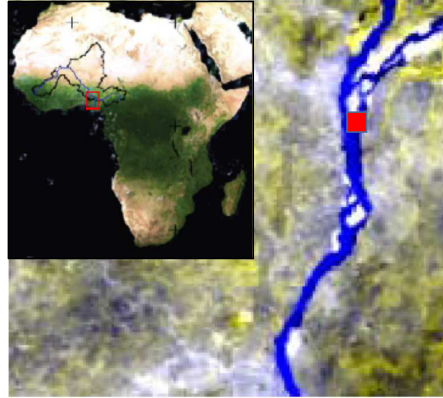
Figure 9: Part of Niger River selected as case study. The location of in situ gauge is also defined by red box

| | Training | | Validation |
	MODIS	in situ	
Simultaneous data approach	2000–2004		2004–2006
Quantile approach	2000–2004	1970–2000	2004–2006

Table 2: Training and validation period for both methods for estimating discharge.

Quantile matching approach

To get rid of the requirement of simultaneous observations, an empirical width-discharge function is defined between their quantile functions instead of themselves directly. The quantile functions of river discharge $Q_Q(p)$ and river width $Q_W(p)$ are defined as followed

$$\begin{aligned} Q_Q(p) &= \inf\{X_Q \in R : p \leqslant F(X_Q)\} \\ Q_W(p) &= \inf\{X_W \in R : p \leqslant F(X_W)\} \end{aligned}$$

Where $F(.)$ is the CDF function and X_Q , X_W refer to the discharge and river width. To eliminate the requirement of synchronous data sets, we try to find a relationship between their quantile functions

$$Q_Q = T(Q_W)$$

This technique is visualized in Figure 11.
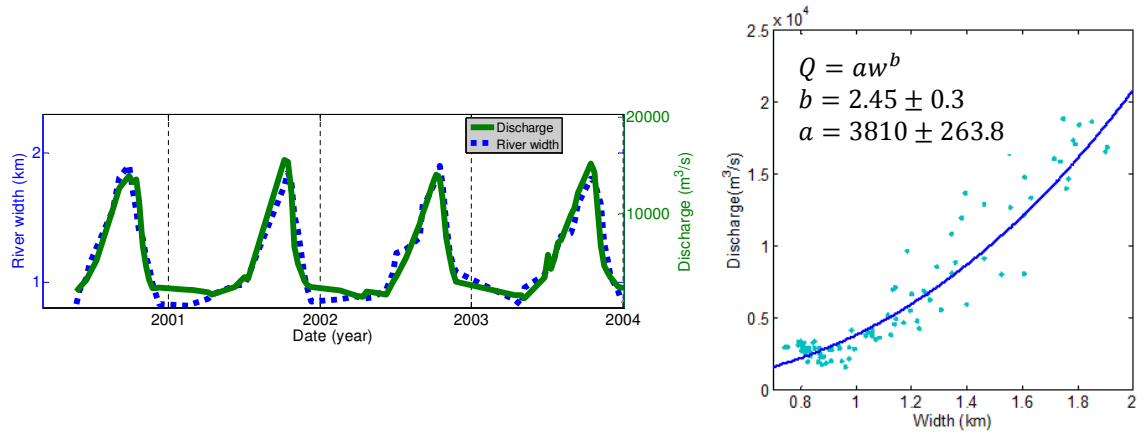
Figure 10: (left) time series of synchronized measurements of discharge and width. (right) scatterplot and the rating curve developed based on it
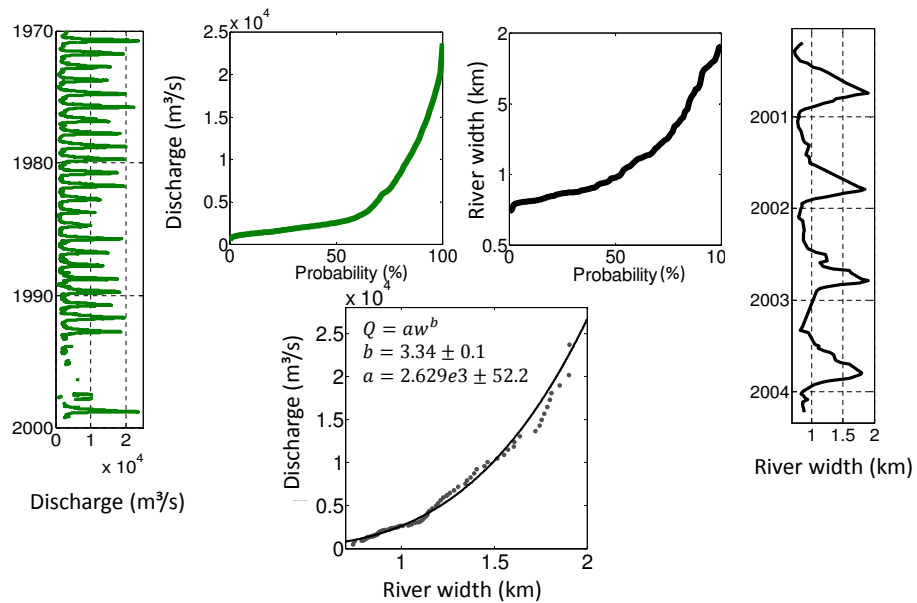
Figure 11: River discharge measurements and river width estimations in two different time frames. Quantile functions of two time series. A power law is fitted to the scatter.
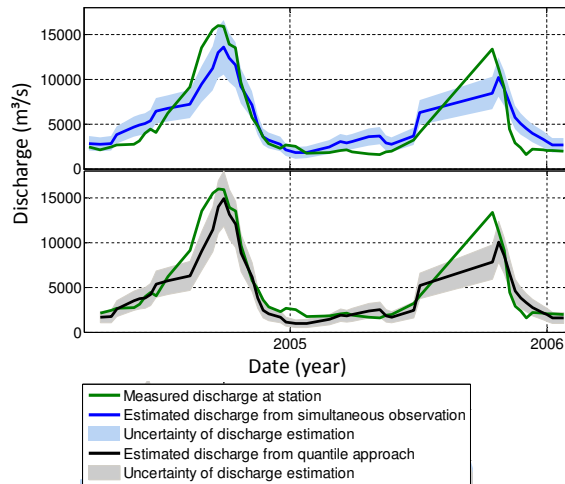
Figure 12: Comparison of estimated and measured river discharge from simultaneous observations approach (up) and quantile approach (down).

At the end, we compare the estimated discharge derived from two presented approaches for the remaining two years, for which in situ observations are available (2004–2006). To do the comparison, we estimate river discharge with its uncertainty using two different empirical relationships. (Figure 12)

To assess the performance of the both approaches to estimate discharge and also validation of results, Root Mean Square Error (RMSE), correlation coefficient and Nash-Sutcliffe modelling efficiency (NSE) are calculated by comparison estimated and measured discharges. By a careful

Approach	Corr.	RMS (%)	NSE
Simultaneous data approach	0.95	13%	0.83
Quantile approach	0.95	11%	0.88

Table 3: Statistical parameters are defined for both approach

look at Table 3, both approaches are able to estimate river discharge with reasonable accuracy (2 times bigger than the in situ observations). Quantile approach performances surprisingly impressive and in respect to the statistical parameters, this technique is able to estimate discharge without using any simultaneous data as accurate as the common method. Since discharge has a

strong stationary behavior over a long time (Figure 11), the quantile matching approach is more successful to estimate discharge than simultaneous data approach as it benefits from more legacy data.

Evaluation of the Performance of Pulse- and Beam-Limited Altimeters for Monitoring Inland Water Bodies

Radar altimeters can be divided into pulse-limited and beam-limited altimeters. The footprint size plays an important role in constructing the return waveform for both altimeter types.

The pulse-limited altimeter employs a nadir-pointing radar to transmit a short pulse with a duration τ of a few nanoseconds. When the trailing edge of the pulse reaches the water surface, the area around the closest approach point would be fully illuminated. The pulse-limited illuminated footprint area can be approximated by a disk with an area of:

$$A = \frac{\pi h c R_{\mathrm{e}}}{h + R_{\mathrm{e}}} \tau \quad , \tag{5}$$

in which h is the satellite altitude, c the speed of light, τ the pulse width and R_{e} is the earth's radius. For the LRM mode of CryoSat-2 the pulse-limited illuminated area is about 2.2 km. Equation (5) says that for a given satellite altitude h the effective footprint area of the return pulse can be controlled by the pulse duration. The whole area inside the footprint contributes to construct the waveform (Figure 13, left middle panel).

Figure 13: Schematic representative of pulse-limited and Doppler beam-limited footprint and waveform

For the beam-limited altimeter type, the shape of the return pulse is dictated by the width of the antenna beam angle. The footprint is defined as the whole area on the earth's surface illuminated by antenna beam angle which depends mainly on antenna gain pattern. The narrow beam width (angle) of the beam-limited altimeters requires a large antenna diameter. Using a synthetic aperture technique and Doppler processing it is possible to reduce the limitation of these altimeters. So this type of altimeters would be Doppler beam-limited.

CryoSat-2 in SAR mode is a Doppler beam-limited altimeter which uses the Doppler beam formation in the along-track direction. In the cross-track direction the illuminated area is similar to that illuminated by pulse-limited altimeters. As Figure 13 shows, in the along-track direction the size of

Figure 15: Water level variation from CryoSat-2 SAR mode and in-situ gauge data

the footprint is very small with respect to its cross-track size. The footprint size of the SAR mode of CryoSat-2 in the along track direction can be calculated from:

$$\Delta x = h\frac{\lambda}{2v}\frac{\text{PRF}}{64} \quad , \tag{6}$$

where λ is the wavelength, v satellite velocity and PRF is the pulse repetition frequency. So for SAR mode of CryoSat-2 the along-track footprint size is just 314 m. However the footprint size in the cross-track direction remains the same size as that of the pulse-limited altimeters.

Figure 14 shows a sequence of 4 illuminating bursts for the pulse- and Doppler beam-limited altimeters which illuminate water surface. In the case of a pulse-limited altimeter there is no overlap between the return burst of pulses because the time interval between pulses is big enough resulting in uncorrelated return pulses. But in Doppler beam-limited altimeter the interval between pulses is too short. Hence the return pulses are cor-

Figure 14: Schematic comparison of illumination from the pulse-limited (left) and Doppler beam-limited (right) altimeters

related. Considering the whole burst as one and doing inter-burst Doppler processing each ground location (Doppler cell) is sensed at multiple times. Each Doppler cell on the ground in the illuminated area is sensed until the satellite moves out of the footprint. Therefore it is possible to reduce the noise.

In this research we analyze the performance of pulse- and beam-limited altimeters for water level monitoring via full- and sub-waveform retracking against available in-situ gauge. To end this, we retracke the full-waveforms and sub-waveforms with different empirical and physical retracking al-
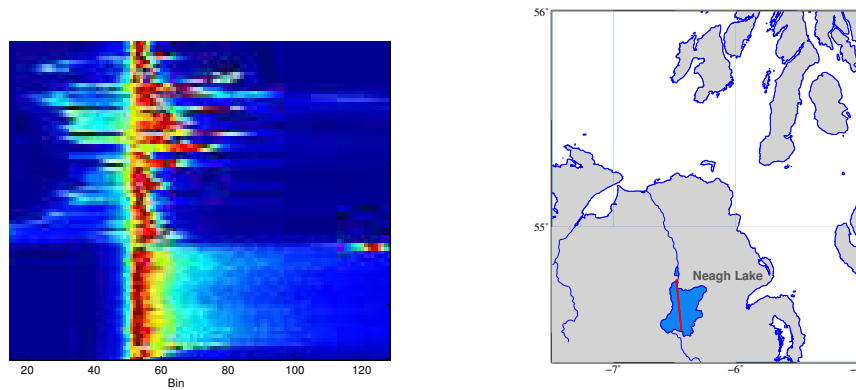
Figure 16: Along track waveform variations for the longest pass of CryoSat-2 SAR mode over Neagh lake, April 2012

Table 4: RMS (cm) of pulse-limited (Envisat) and Doppler beam-limited altimeter (CryoSat-2 SAR mode) water level from different retrackers (Neagh lake)

retracker	full-waveform	sub-waveform		
		first	mean-all	min-res
Envisat ice-1	32	–	–	–
CryoSat-2 GS	18	–	–	–
5β-parameters	19	48	74	77
OCOG	20	48	38	88
Threshold 10%	19	21	**11**	22
Threshold 20%	62	32	12	26
Threshold 50%	22	47	17	24
SAMOSA3	**15.5**	**13**	–	–

gorithms such as OCOG, threshold, β-parameters and SAMOSA3. The result of our data analysis are shown in Table 4 and Figure 15.

Theses

(http://www.gis.uni-stuttgart.de/research/dissertations/)

Chen Q: Analyzing and modeling environmental loading induced displacements with GPS and GRACE. DGK, series C, volume 752

Devaraju B: Understanding filtering on the sphere - Experiences from filtering GRACE data. DGK, series C, volume 756

Diploma/Master Theses

(http://www.gis.uni-stuttgart.de/edu/theses/finished_theses/)

Omid Elmi: The role of multispectral image transformations in change detection

Shakti Gahlaut: Determination of surface water area using multitemporal SAR imagery

Shirzad Roohi: Capability of pulse-limited satellite radar altimetry to monitor inland water bodies

Sadegh Modiri: Copula-based analysis of correlation structures in case of GRACE coefficients

Bachelor Theses

(http://www.gis.uni-stuttgart.de/edu/theses/finished_theses/)

Alexander Walton: Assessing the performance of different classification methods to detect inland surface water extent

Peter Hurt: Untersuchung von Schweredifferenzen durch Punktmassenmodellierung anhand der GRACE-Schwerefelddaten eines Gletschergebiets

Ganyi Wang: Noise characterization of GPS time series from the second IGS reprocessing campaign

Publications

(http://www.gis.uni-stuttgart.de/research/publications/)

Refereed Journal Publications

Ghobadi-Far, K., M. Sharifi, and N. Sneeuw (2015). *GOCE gradiometry data processing using the Rosborough approach. J. Geodesy* 89.12, pp. 1245–1261. DOI: 10.1007/s00190-015-0849-6.

Grafarend, E. W. (2015a). *The reference figure of the rotating Earth in geometry and gravity space and an attempt to generalize the celebrated Runge-Walsh approximation theorem for irregular surfaces. International Journal on Geomathematics* 6 (2), pp. 101–140. DOI: 10.1007/s13137-014-0068-y.

Grafarend, E. W. and R.-J. You (2015). *Fourth order Taylor-Kármán structured covariance tensor for gravity gradient predictions by means of the Hankel transformation. International Journal on Geomathematics* 6 (2), pp. 319–342. DOI: DOI10.1007/s13137-015-0071-y.

Keller, W. and R.-J. You (2015). *Rosborough approach for the determination of regional time variability of the gravity field from satellite gradiometry data. GEM International Journal on Geomathematics* 6 (2), pp. 295–318. DOI: 10.1007/s13137-015-0077-5.

Lorenz, C., M. J. Tourian, B. Devaraju, N. Sneeuw, and H. Kunstmann (2015b). *Basin-scale runoff prediction: An Ensemble Kalman Filter framework based on global hydrometeorological data sets. Water Resources Research* 10, pp. 8450–8475. DOI: 10.1002/2014WR016794.

Other Refereed Contributions

Roese-Koerner, L., B. Devaraju, W. D. Schuh, and N. Sneeuw (2015). *Describing the Quality of Inequality Constrained Estimates*. In: *The 1st International Workshop on the Quality of Geodetic Observation and Monitoring System (QuGOMS'11)*. (Apr. 13–15, 2011). Ed. by H. Kutterer, F. Seitz, H. Alkhatib, and M. Schmidt. Vol. 140. IAG Symposia. IAG International Workshop, Munich, Germany: Springer Verlag, pp. 15–20. DOI: 10.1007/978-3-319-10828-5_3.

Tourian, M. J., R. Thor, and N. Sneeuw (2015). *Least-Squares Prediction of Runoff Over Ungauged Basins*. In: *International Association of Geodesy Symposia*. Ed. by C. Rizos and P. Willis. Springer Berlin Heidelberg, pp. 1–5. DOI: 10.1007/1345_2015_170.

Poster Presentations

Antoni, M., W. Keller, T. Kersten, and S. Schön (2015). *Alternative GNSS antenna calibration in terms of Bernstein-Bezier polynomials*. IUGG 2015 General Assembly, Prag.

Birang, M. and S. Roohi (2015). *Monitoring subsidence of metro network from InSAR*. IUGG, Prague, Czech Republic.

Chen, Q., B. Cui, and N. Sneeuw (2015). *Singular spectrum analysis for modelling geodetic time series*. IUGG, Prague, Czech Republic.

Chen, Q., T. van Dam, Z. Li, L. Wang, and N. Sneeuw (2015). *On modeling the environmental loading induced displacements in the local area*. IUGG, Prague, Czech Republic.

Devaraju, B. and N. Sneeuw (2015b). *On the spatial resolution of filters defined on the sphere*. IUGG, Prague, Czech Republic.

Elmi, O., M. J. Tourian, and N. Sneeuw (2015b). *Improving the temporal and spatial resolution of water level time series over Po River (Italy) obtained by satellite altimetry*. IGARSS 2015, Milan, Italy.

Elmi, O., M. J. Tourian, and N. Sneeuw (2015d). *Comparison of different automatic adaptive threshold selection techniques for estimating discharge from river width*. EGU General assembly 2015, Vienna, Austria.

Iran Pour, S., T. Reubelt, N. Sneeuw, and ESA SC4MGV Study Team (2015). *Impact of groundtrack pattern of double pair missions on the gravity recovery quality – Lessons from the ESA SC4MGV project*. IUGG, Prague, Czech Republic.

Keller, W. (2015a). *Data mining in GRACE monthly solutions (solicited)*. European Geosciences Union General Assembly 2015, Vienna, Austria.

Keller, W. (2015b). *Data mining in SST monthly solutions*. 26th IUGG general Assembly 2015, Prague, Czech Republik.

Li, H., M. Antoni, T. Reubelt, Z. Zhou, M. Zhong, Q. Chen, and N. Sneeuw (2015). *A Semi-analytical Approach to Gravity Field Analysis from Pendulum Formation*. IUGG 2015 General Assembly, Prague, Czech Republic.

Liu, W., S. Iran Pour, M. J. Tourian, T. Reubelt, and N. Sneeuw (2015). *Impact of satellite repeat period and gravity recovery resolution on ocean tide aliasing periods*. Geodätische Woche, Stuttgart, Germany.

Modiri, S., S. Iran Pour, C. Lorenz, H. Kunstmann, and N. Sneeuw (2015). *Copula-based filtering for GRACE Follow-On and future satellite gravity missions*. IUGG, Prague, Czech Republic.

Modiri, S., C. Lorenz, N. Sneeuw, and H. Kunstmann (2015). *Copula-based estimation of large-scale water storage changes: exploiting the dependence structure between hydrological and GRACE data*. EGU, Vienna, Austria.

Roth, M., M. Antoni, B. Devaraju, M. Weigelt, and N. Sneeuw (2015). *SHBundle – spherical harmonic synthesis/analysis until very high degree/order*. Geodetic Week, Stuttgart, Germany.

Sharifi, M. A., K. Ghobadi-Far, and N. Sneeuw (2015). *Representation of the geopotential functionals based on a 2D Fourier expression in terms of spherical coordinates*. Geodätische Woche, Stuttgart, Germany.

Sneeuw, N., Q. Chen, and B. Cui (2015). *On the capabilities of singular spectrum analysis for modeling geodetic time series*. Geodätische Woche, Stuttgart, Germany.

Sneeuw, N., K. Ghobadi-Far, and M. A. Sharifi (2015). *Analysis of GOCE gravitational gradients by the Rosborough formulation*. Geodätische Woche, Stuttgart, Germany.

Tourian, M. J., A. Tarpanelli, O. Elmi, T. Qin, L. Brocca, T. Moramarco, and N. Sneeuw (2015). *River discharge estimation along the Po river from densified water level time series of multi-mission satellite altimetry spatially and temporally*. Third Space for Hydrology Workshop, ESA-ESRIN, Frascati, Italy.

Vishwakarma, B. D. and N. Sneeuw (2015). *Importance of leakage analysis for trend studies.* Geodätische Woche, Stuttgart, Germany.

Wang, L., T. van Dam, M. Weigelt, M. J. Tourian, Q. Chen, and N. Sneeuw (2015). *Continental water storage variations inferred from 3-D GPS coordinates timeseries for the major river basins in Europe and North America.* IUGG, Prague, Czech Republic.

Zhang, J. and N. Sneeuw (2015a). *Predicting the variation of continental water storage by ENSO index.* IUGG, Prague, Czech Republic.

Zhang, J. and N. Sneeuw (2015b). *Statistical investigation of sensitivity of river discharge and continental total water storage with respect to ENSO.* Geodätische Woche, Stuttgart, Germany.

Conference Presentations

Aghakouchak, A. and M. J. Tourian (2015). *Multi-Sensor Drought Monitoring, Prediction and Recovery Assessment Using Gravimetry Information.* EGU2015, Vienna, Austria.

Antoni, M., H. Li, T. Reubelt, and N. Sneeuw (2015). *Pre-mission error assessment for the pendulum formation via the semi-analytical approach.* Geodätische Woche/Intergeo 2015, Stuttgart.

Daras, I., R. Pail, P. Visser, M. Weigelt, S. Iran Pour, M. Murböck, T. Gruber, J. Texeira da Encarnação, N. Sneeuw, S. Tonetti, S. Christian, J. van den IJssel, S. Cornara, T. van Dam, S. Cesare, and R. Haagmans (2015). *Temporal aliasing effects on future gravity satellite missions and their assessment – Lessons from the ESA-SC4MGV project.* EGU, Vienna, Austria.

Devaraju, B. and N. Sneeuw (2015a). *Insights into filtering on the sphere offered by the polar form of spherical harmonics.* EGU 2015, Vienna, Austria.

Domeneghetti, A., A. Tarpanelli, M. J. Tourian, L. Brocca, T. Moramarco, A. Castellarin, and N. Sneeuw (2015). *Hydraulic model calibration by using satellite altimetry: comparison of different products.* Third Space for Hydrology Workshop, ESA-ESRIN, Frascati, Italy.

Elmi, O., M. J. Tourian, and N. Sneeuw (2015a). *A comparison between Landsat and MODIS images for estimating discharge from river width.* 36th International Symposium on Remote Sensing of Environment (ISRSE36), Berlin, Germany.

Elmi, O., M. J. Tourian, and N. Sneeuw (2015c). *An automatic water body area monitoring algorithm for satellite images based on Markov Random Fields.* Geodetic Week 2015, Stuttgart, Germany.

Elmi, O., M. J. Tourian, and N. Sneeuw (2015e). *River discharge estimation using effective width: a comparison between Landsat and MODIS imagery.* ISRSE36, Berlin, Germany.

Elmi, O., M. J. Tourian, and N. Sneeuw (2015f). *River discharge estimation using effective width: a comparison between Landsat and MODIS imagery*. Third Space for Hydrology Workshop 2015, ESA-ESRIN, Frascati, Italy.

Iran Pour, S., M. Weigelt, T. Reubelt, I. Daras, M. Murböck, J. Teixeira da Encarnaç ao, J. van den IJssel, S. Tonetti, S. Cornara, S. Cesare, T. Gruber, T. van Dam, P. Visser, R. Pail, N. Sneeuw, L. Massotti, C. Siemes, and R. Haagmans (2015). *Study of post-processing methods for future gravity satellite missions*. IUGG, Prague, Czech Republic.

Lin, Y., J. Yu, M. Shen, J. Cai, and N. Sneeuw (2015). *The Spatio-temporal Dynamic Analysis of Wetland Evolution Process in Chongming Dongtan Using Remote Sensing Data*. IUGG, Prague, Czech Republic.

Liu, W., S. Iran Pour, M. J. Tourian, and N. Sneeuw (2015). *De-aliasing of ocean tide error in future dual-pair satellite gravity missions*. IUGG, Prague, Czech Republic.

Lorenz, C., M. J. Tourian, B. Devaraju, N. Sneeuw, and H. Kunstmann (2015a). *Prediction of basin-scale runoff using an Ensemble Kalman filter framework based on global hydrometeorological datasets*. IUGG, Prague, Czech Republic.

Riegger, J. and M. J. Tourian (2015). *Operational Forecast of Runoff from Large Scale Basins using Satellite Gravimetry and Remote Sensing*. EGU2015, Vienna, Austria.

Roohi, S. and N. Sneeuw (2015). *River monitoring from multi satellite altimetry missions, Earth observation for water cycle science*. Third Space for Hydrology Workshop, ESA-ESRIN, Frascati, Italy.

Roohi, S., N. Sneeuw, S. Dinardo, and J. Beneviste (2015a). *Evaluation of CryoSat-2 performance over inland water bodies*. IUGG, Prague, Czech Republic.

Roohi, S., N. Sneeuw, S. Dinardo, and J. Beneviste (2015b). *Monitoring of lake water level variation from pulse and doppler beam-limited altimeters*. Geodätische Woche, Stuttgart, Germany.

Schlesinger, R. (2015). *Sensorcheck am CG-5*. 5. Erfahrungsaustausch der Scintrex CG-5 Anwender, Stuttgart, Germany.

Tourian, M. J. and N. Sneeuw (2015). *A Kalman Filter approach to estimate river discharge using altimetric water level time series*. Third Space for Hydrology Workshop 2015, ESA-ESRIN, Frascati, Italy.

Tourian, M. J., T. Qin, O. Elmi, A. Tarpanelli, L. Brocca, T. Maramarco, and N. Sneeuw (2015). *Improving the temporal and spatial resolution of water level time series over Po River (Italy) obtained by satellite altimetry*. IGARSS 2015, Milan, Italy.

Vishwakarma, B. D., B. Devaraju, and N. Sneeuw (2015a). *Data driven approach to minimize effects of filtering on GRACE*. Geodätische Woche, Stuttgart, Germany.

Vishwakarma, B. D., B. Devaraju, and N. Sneeuw (2015b). *Minimizing signal loss due to filtering of GRACE observed total water storage change*. IUGG, Prague, Czech Republic.

Books & Miscellaneous

Grafarend, E. W. (2015b). "Theory of Map Projections: From Riemann to Riemann Manifolds". In: *Handbook of Geomathematics*. Ed. by W. Freeden, Z. M. Nashed, and T. Sonar. Springer Verlag, Berlin-Heidelberg, pp. 1–69. DOI: 10.1007/978-3-642-27793-1_53-1.

Grafarend, E. W., M. Klapp, and Z. Martinec (2015). "Spacetime modeling of the Earth's gravity field by ellipsoidal harmonics". In: *Handbook of Geomathematics*. Ed. by W. Freeden, Z. M. Nashed, and T. Sonar. 2nd edition. Springer Verlag, Berlin-Heidelberg, pp. 381–456.

Keller, W. (2015c). "Satellite-to-Satellite Tracking (Low-Low/High-Low SST)". In: *Handbook of Geomathematics*. Ed. by W. Freeden, Z. Nashed, and T. Sonar. Springer-Verlag, Berlin Heidelberg, pp. 171–210. ISBN: 978-3-642-54551-1.

Guest Lectures and Lectures on special occasions

J. Flury (Institut für Erdmessung, Leibniz Universität Hannover): Relativistische Geodäsie und Gravimetrie mit Quantensensoren (9.1.)

R. Dietrich (Institut für Planetare Geodäsie, TU Dresden): Die Eismassenbilanz großer kontinentaler Eisschilde aus geodätischer Perspektive (6.11.)

Research Stays

Grafarend E.:
Finnish Geodetic Research Institute, Masala/Helsinki, Finland (11.8. – 1.9.)

Lecture Notes

(http://www.gis.uni-stuttgart.de/edu/study/bscgug/,
http://www.gis.uni-stuttgart.de/edu/study/mscgug/,
http://www.gis.uni-stuttgart.de/edu/study/mscgeo/)

Grafarend E. W. and F. Krumm:
Kartenprojektionen (Map Projections), 236 pages
Keller W.:
Foundations of Satellite Geodesy, 51 pages
Foundations of Satellite Geodesy (Viewgraphs), 281 pages
Observation Techniques in Satellite Geodesy, 211 pages

Krumm F.:
>   Map Projections and Geodetic Coordinate Systems, 236 pages
>   Mathematical Geodesy (Landesvermessung), 170 pages
>   Reference Systems (Referenzsysteme), 174 pages

Sneeuw N.:
>   Geodesy and Geoinformatics, Part Geodesy, 31 pages
>   History of Geodesy, 38 pages
>   Physical Geodesy, 137 pages

Sneeuw N., Krumm F. and Roth M.:
>   Adjustment Theory, 155 pages

University Service

Grafarend E.
>   Member Faculty of Aerospace Engineering and Geodesy
>   Member Faculty of Civil- and Environmental Engineering
>   Member Faculty of Mathematics and Physics

Keller W.
>   Associate Dean (Academic) Geodäsie & Geoinformatik and GeoEngine, Stuttgart

Roth M.
>   Member/chairman of the PR-committee of the study course Geodesy & Geoinformatics
>   Member of the appointments committee "Photogrammetry, Remote Sensing and Geoinformatics"

Sneeuw N.
>   Search Commitee Statik and Dynamik der Luft- und Raumfahrtkonstruktionen
>   Search Committee Romanische Literaturen, Senate Reporter
>   Search Committee Navigation und geodätische Schätzverfahren
>   Search Committee Photogrammetrie, Fernerkundung und Geoinformation
>   Stand-by Member Senate Committee for Structural Development and Research, Stuttgart

Professional Service (National)

Grafarend E. Emeritus Member German Geodetic Commission (DGK)

Sneeuw N.
>   Full Member Deutsche Geodätische Kommission (DGK)
>   Chair DGK section "Erdmessung", until 25.11.15
>   Member Scientific Board of DGK, until 25.11.15

Professional Service (International)

Grafarend E.
  Professor h.c., University of Navarra, Pamplona, Spain
  Elected Member of the Finnish Academy of Sciences and Letters, Finland
  Elected Member of the Hungarian Academy of Sciences, Hungary
  Member Royal Astronomical Society, Great Britain
  Corresponding Member Österreichische Geodätische Kommission (ÖGK)
  Member Flat Earth Society
  Elected Member Leibniz-Sozietät, Berlin
  Fellow International Association of Geodesy (IAG)

Sneeuw N.
  Adjunct Professor of the College of Engineering, University of Tehran, 03.2015–02.2017
  President IAG InterCommission Committee on Theory (ICCT), until 07.2015
  Member Editorial Board of Studia Geophysica et Geodaetica
  Member Editorial Board of Surveys in Geophysics
  Fellow International Association of Geodesy (IAG)
  Member Assessment Panel Space Research, NWO, Netherlands

Courses – Lecture/Lab/Seminar

Advanced Mathematics (Keller, Antoni)	3/2/0/0
Aktuelle Geodätische Satellitenmissionen (Sneeuw)	2/2/0/0
Amtliches Vermessungswesen und Liegenschaftskataster (Steudle)	2/0/0/0
Amtliche Geoinformation (Heß)	2/0/0/0
Ausgewählte Kapitel der Parameterschätzung (Krumm, Roth)	2/2/0/0
Ausgleichungsrechnung I, II (Krumm, Roth)	3/1/0/0
Dynamische Erdmodelle (Tourian)	0/2/0/0
Dynamische Satellitengeodäsie (Sneeuw, Tourian)	1/1/0/0
Einführung Geodäsie und Geoinformatik (Sneeuw)	2/2/0/0
Foundations of Satellite Geodesy (Keller)	2/1/0/0
Integriertes Praktikum/Integrated Field Work (Keller, Sneeuw)	10 days
Koordinaten- und Zeitsysteme in der Geodäsie (Sneeuw)	2/2/0/0
Landesvermessung (Krumm, Roth)	2/2/0/0
Map Projections and Geodetic Coordinate Systems (Krumm, Roth)	2/1/0/0
Physikalische Geodäsie (Engels, Tourian)	2/2/0/0
Referenzsysteme (Krumm, Roth)	2/2/0/0
Satellitengeodäsie (Sneeuw, Tourian)	2/1/0/0
Satellitengeodäsie (Keller, Tourian)	1/1/0/0
Satellite Geodesy Observation Techniques (Keller, Tourian)	2/1/0/0

Statistical Inference (Krumm, Roth) 2/1/0/0
Wertermittlung I, II (Bolenz) 4/0/0/0

Institute of Navigation

Breitscheidstrasse 2, D-70174 Stuttgart,
Tel.: +49 711 685 83400, Fax: +49 711 685 82755
e-mail: ins@nav.uni-stuttgart.de
homepage: http://www.nav.uni-stuttgart.de

Head of Institute

Prof. Dr.-Ing. Alfred Kleusberg

Deputy: Dr.-Ing. Aloysius Wehr
Secretary: Helga Mehrbrodt

Staff

Dipl.-Ing. Doris Becker	Navigation Systems
Dipl.-Ing. Michael Gäb	Navigation Systems
Dipl.-Geogr. Thomas Gauger	GIS Modelling and Mapping
Dipl.-Ing. Marc Goetzke	GIS Modelling and Mapping
Dipl.-Ing. René Pasternak	Remote Sensing
Dipl.-Ing. Bernhardt Schäfer	Navigation Systems
M. Sc. Hendy Suhandri	Navigation Systems
Dipl.-Ing. (FH) Martin Thomas	Laser Systems
Dr.-Ing. Aloysius Wehr	Laser Systems
Dr. Ing. Franziska Wild-Pfeiffer	Navigation Systems

EDP and Networking

Regine Schlothan

Laboratory and Technical Shop (ZLW)

Dr.-Ing. Aloysius Wehr (Head of ZLW)
Technician Peter Selig-Eder
Electrician Sebastian Schneider
Mechanician Master Michael Pfeiffer

External teaching staff

Hon. Prof. Dr.-rer.nat. Volker Liebig - Directorate ESA
Hon. Prof. Dr.-Ing. Hans Martin Braun - RST Raumfahrt Systemtechnik AG, St.Gallen
Dr. Werner Enderle - Europäisches Satelliten Kontrollzentrum (ESOC), Darmstadt

Research Projects

Experimental 3D Printer for Case Production and Printing 3D Laser Scanner Data

As 3D printing has become more and more a common tool for prototype manufacturing, the ZLW decided that 3D printing can ease especially the case manufacturing for small electronic navigation sensors and systems. Up to now, aluminum cases have been milled in the workshop. However, the INS has been involved in research projects in recent years which have been focused on the development of wearable sensor systems. Here small plastic packages have been required, because they are light-weight and more comfortable in wearing. In a first approach plastic boxes were bought off the shelf. But their dimensions did not fit and additional machining was required. Therefore, it was figured out, that 3D printing improves the production of special miniature cases. In order to obtain expert knowledge about the hard- and software configuration and key parameters of 3D printers, it was concluded not to buy printer and software off the shelf but to design and to build up an Experimental 3D Printer (E3DP) by the personal of ZLW and research assistants. The design objective was that E3DP should perform an accuracy better than one tenth of a millimeter using poly-lactic acid (PLA) as printing material and the maximum possible printed volume should be 300 mm x 300 mm x 200 mm (length x width x height). The mechanical setup was designed and built up by ZLW. The printer comprises an Extruder Bulldoc with Merlin Hotend as printing head and control electronics realized by Ramps 1.4 (RepRap Arduino Mega Pololu Shield) running Repetier firmware. STL (STereoLithography, Standard Tessellation Language) files are required for printing. This format is a standard output interface of e.g. CAD programs. The STL files are further processed by the program Repetier-Host V.1.60 with subprogram Slic3r on a PC. Both routines are open source software. The output of Repetier-Host V.1.60 is sent to E3DP for 3D printing via USB.

Figure 1 shows the extruder head during printing of a test object. In a second step data sets obtained by laser scanning digitization were printed. The data of the 3D Laser Scanner (3D-LS) were transformed into STL format, sliced by Repetier-Host V1.60 and printed by E3DP (s. Figure 2). Finally small boxes for wearable electronics were printed on the basis of CAD data (s. Figure 3).

The carried out experiments make clear, that 3D printing is an ideal tool for the jobs carried out by the workshop (ZLW) in the course of studies Geodesy & Geoinformatics. Plastic cases and plastic spare parts can be printed using either CAD data or 3D data sampled by 3D digitization systems e.g. 3D laser scanners. ZLW learned that commercial preprocessing and slicing software is advisable, if an operational production is envisaged.
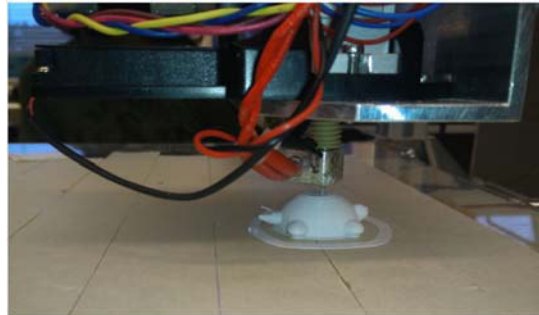
Figure 1: Print head with extruder.
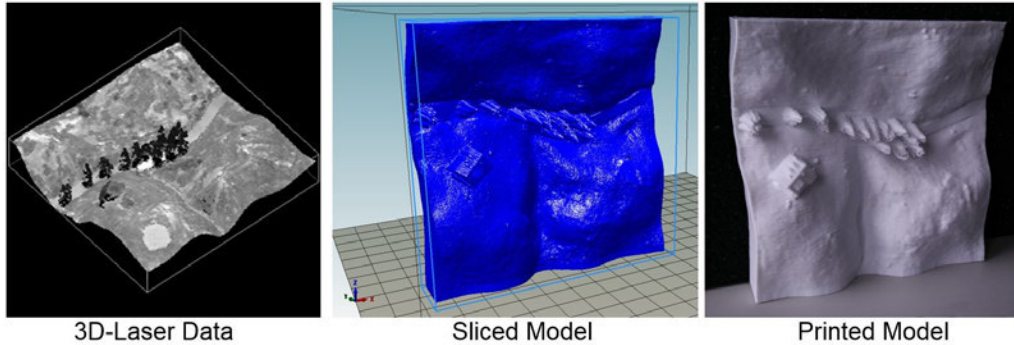
Figure 2: Printing 3D laser scanner data.

Figure 3: Printed case.

GPOS-Bl Demonstration Setup for Education and Exhibitions

In recent years the INS developed a low-cost Positioning and Orientation System called General Purpose Position and Orientation Sensor Box light (GPOS-Bl), which comprises a ublox-GPS/EGNOS receiver and a MEMS-IMU. In this box proprietary software is run on a PC compatible computer board computing first three dimensional positions out of the receivers GPS/EGNOS raw data and then calculating an integrated solution for the 3D position and orientation angles of the platform by processing the computed GPS/EGNOS position and the IMU measurement data in a Kalman filter. The technical data are compiled in Table 1. This measurement box is primarily applied in education for recording flight trajectories during test and practice flights. However, it is also used in surveying with airborne low-cost remote sensing equipment and can be applied as a sensor for approach and landing aids for small and medium sized airplanes in general and business aviation.

GPS	ublox LEA6
IMU	ADIS 1636
output	CF-Memory Card, RS 232, PPS (TTL)
data	position, velocity, orientation angles, GPS week seconds
accuracy	position: < 3 m orientation angles: < 0.1°
measurement rate	max. 50 Hz
power supply	9 V - 36 V

Table 1: Technical data of GPOS-Bl.

Figure 4 depicts that GPOS-Bl is only a box which delivers the user a serial data stream either on CF-memory card or via the serial interface RS 232 for later processing in dependence on the application. In order to make this product an eye-catcher on exhibitions and an interesting demonstration item for students, this measurement system was redesigned and extended by a display. Now, the instantaneous measurement data position and orientation are displayed on the box. Especially the orientation angles are visualized by an artificial horizon. This advanced GPOS-Bl was mounted on a model airplane to demonstrate the real-time performance of the measurement system (s. Figure 5). This setup was exhibit at the INTERGEO 2015 trade fare for Geodesy, Geoinformation and Land Management in Stuttgart.

Figure 4: GPOS-BI.

Figure 5: Advanced GPOS-BI mounted on a model airplane.

Inertial Measurement Units and Integrated INS/GNSS Systems Based on Consumer-Grade MEMS Components for Sport Monitoring, Indoor Navigation and Land Vehicle Navigation

Applications in sport monitoring and pedestrian indoor navigation require stand alone and miniature inertial measurement units and data loggers with the same specifications in size and sensor characteristics. New wireless prototypes have been designed by TGU LOPSTRE navigation to sense several types of movements via synchronised Bluetooth data transfer without cables. The cases were printed with the Experimental 3D Printer (E3DP) available at the Institute of Navigation. In the cases with the dimensions (39 x 26 x 17) mm, a rechargeable battery for measurements for up to three hours can be fitted under the PCB carrying the sensor, microcontroller and communications devices. Figure 6 shows the CAD design, a complete unit with transparent cover plate, the side view of a PCB with battery and an empty 3D printed case (from left to right).

Figure 6: Wearable MEMS inertial sensors with rechargeable battery and Bluetooth module in 3D printed case.

For the application of land vehicle navigation, a Raspberry Pi MEMS inertial sensor extensions board was equipped with the L1 GNSS module NV08C-CSM v.4.1 from NVS Technologies. The extension board was originally designed by TGU LOPSTRE *navigation* to be used for data logging in figure skating. Figure 7 shows the consumer-grade integrated inertial navigations system attached to the mounting plate at the van of the Institute of Navigation. The low-cost unit was used in several drives and the performance was compared to the integrated inertial navigation system Applanix LV420 in a master thesis.

Figure 7: Consumer-grade integrated inertial navigation system.

Analysis and Correction of Data Sets of Nitrogen Deposition in Baden-Württemberg Contributing to a Country Specific Nitrogen Balance

On behalf and on the account of Baden-Württemberg the project „Application of modelled nitrogen deposition 2007/2009 for ecosystems in Baden-Württemberg" is carried out. The results of the research BMU/UBA project „PINETI 2" (Pollutant Input and EcosysTem Impact; BMU/UBA FE-No 3712 63 240-1), are compiled, analysed and corrected within this project.

Since the latest „PINETI 2" modelling results of anthropogenic nitrogen dry deposition, modelled using the chemical transport model LOTOS-EUROS, are severely underestimating measurements of total nitrogen input into forest ecosystems in Baden-Württemberg, it was decided to develop and apply a methodology to correct „PINETI2" deposition data fields in order to be in line with empirical „ground truth" data based on measurements available at more than 20 forest plots in Baden-Württemberg.

The correction procedure is carried out using geo-statistical GIS application in order to derive high resolution maps of ecosystem specific nitrogen deposition. In south-west Germany the complex orographic situation is to a greater extent determining the magnitude of nitrogen total deposition on a small scale. The co-kriging technique used enables accounting for these local phenomena by making use of high resolution digital elevation model data together with high quality deposition data measured at 20 forest plots in Baden-Württemberg when deriving nitrogen deposition maps. The resulting maps are in 100 x 100 m^2 grid resolution.
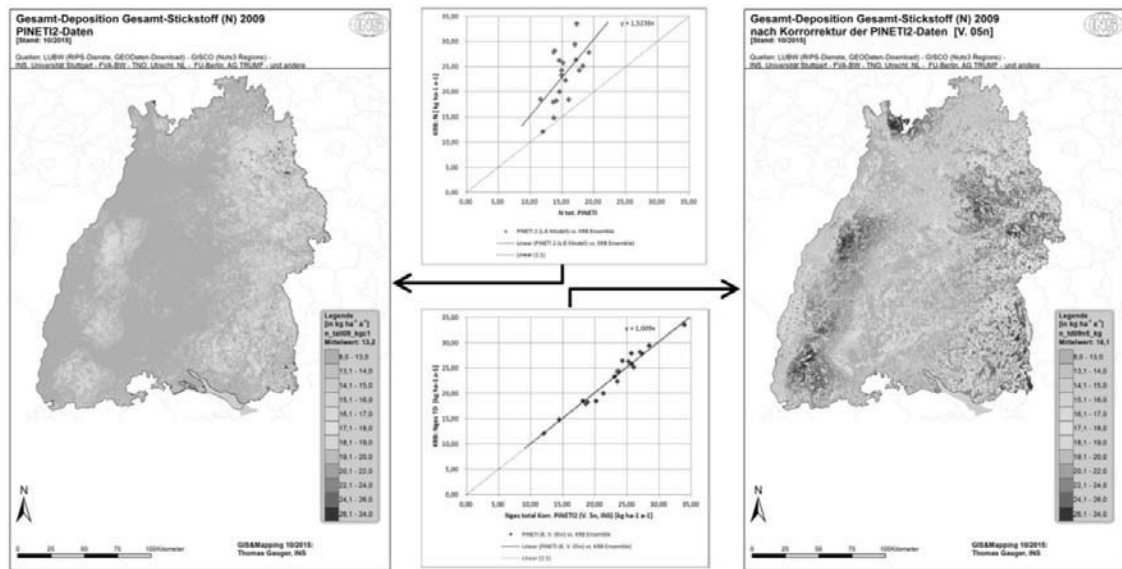
Figure 8: Total deposition of reactive nitrogen in Baden-Württemberg 2009: BMU/UBA PINETI model output (left); map corrected using forest measurement data (right); the scatter plots (middle) are indicating the respective quality of the map (x-axis) with respect to empirical N deposition estimates at coniferous forest plots (y-axis).[Data Sources: BMU/UBA 37126340-1, FVA-BW LUBW and others]

Within the project national nitrogen deposition maps (Figure 8, left) are corrected and high resolution maps of ecosystem specific nitrogen deposition fluxes are generated for Baden-Württemberg (see Figure 8, right). The resulting data of this project are delivered as one data base amongst others for further calculation of a comprehensive nitrogen balance for Baden-Württemberg. The data will be made accessible via internet at LUBW (StickstoffBW online) in order to be used for different research projects in the field of ecological impact assessment, biodiversity, and nature protection. Administrative applications aiming at emission control and emission reduction of air pollutants are using the mapped nitrogen deposition data with reference to permission of projected animal husbandry, road construction, industrial settlements, and power plants, respectively.

Publications and Presentations

Schäfer, B.; Wild-Pfeiffer, F.: IMU - Moderne Hybridsensorik - Entwicklung und Stand der Technik, In: Arampatzis, A. (Ed.), Schriften der Deutschen Vereinigung für Sportwissenschaft; Jahrestagung der dvs-Sektion Biomechanik vom 26.-28. März 2015 in Berlin., Feldhaus, Edition Czwalina, 2015, 252, 93-97

Bachelor Thesis

Empirische Bewertung von Akquisitionsverfahren für GALILEO E1 Signale (Supervisor: Dr.-Ing. A. Wehr)

Erfassung von Algen in Gewässern mittels Methoden der Fernerkundung (Supervisor: Dipl.-Geogr. R. Pasternak)

Untersuchung zweier Teilaspekte zu MEMS-Inertialsensoren (Supervisor: Dr.-Ing. F. Wild-Pfeiffer)

Analyse der Stadtentwicklung Addis Abebas von 1972 bis 2015 unter Nutzung von Fernerkundungsdaten (Supervisor: Dipl.-Geogr. R. Pasternak)

Untersuchung der g-Sensitivität bei MEMS-Drehratensensoren (Supervisor: (Dr.-Ing. F. Wild-Pfeiffer, Dipl.-Ing. B. Schäfer)

Beobachtungen von Veränderungen entlang der ehemaligen innerdeutschen Grenzen zwischen Sachsen und Bayern zwischen 1985 und 2015 (Supervisor: Dipl.-Geogr. R. Pasternak)

Master Thesis

Untersuchungen zur PPP-Performance eines Low-cost-GNSS-Empfängers im Bereich kinematischer Anwendungen (Supervisor: Dipl.-Ing. B. Becker)

Datenerfassung, Synchronisierung und Implementierung eines integrierten low-cost INS/GNSS Navigationssystems (Supervisor: Dipl.-Ing. B. Schäfer)

Precise Orbit Determination for Satellite Formations and Constellations (Supervisor: Dr.-Ing. W. Enderle)

Activities in National and International Organizations

Alfred Kleusberg
Fellow of the International Association of the Geodesy
Member of the Institute of Navigation (U.S.)
Member of the Royal Institute of Navigation
Member of the German Institute of Navigation

Education (Lecture / Practice / Training / Seminar)

Introduction of Geodesy and Geoinformatic (BSc) (Kleusberg, Schäfer)	2/2/0/0
Electronics and Electrical Engineering (Wehr)	2/1/0/0
Satellite Measurement Engineering (Wehr)	2/1/0/0
Parameter Estimation in Dynamic Systems (Kleusberg, Gäb)	2/1/0/0
Navigation I (Kleusberg, Gäb, Becker)	2/2/0/0
Inertial Navigation (Kleusberg, Schäfer)	2/2/0/0
Remote Sensing I (Wild-Pfeiffer, Pasternak)	2/2/0/0
Remote Sensing I (BSc) (Wild-Pfeiffer, Pasternak)	2/1/0/0
Remote Sensing II (Wild-Pfeiffer, Pasternak)	1/1/0/0
Satellite Programs in Remote Sensing, Communication and Navigation I (Liebig)	2/0/0/0
Satellite Programs in Remote Sensing, Communication and Navigation II (Liebig)	2/0/0/0
Radar Measurement Methods I (Braun)	2/0/0/0
Radar Measurement Methods II (Braun)	2/1/0/0
Dynamic System Estimation (Kleusberg, Gäb)	2/1/0/0
Integrated Positioning and Navigation (Kleusberg, Suhandri, Schäfer)	2/1/0/0
Satellite Navigation (Kleusberg, Suhandri, Gäb)	2/1/0/0
Interplanetary Trajectories (Becker)	1/1/0/0
Geodetic Seminar I, II (Fritsch, Sneeuw, Keller, Kleusberg, Schwieger)	0/0/0/4
Integrated Fieldwork (Pasternak, Schäfer)	(SS 2015)

Institute for Photogrammetry

Geschwister-Scholl-Str. 24D, D-70174 Stuttgart
Tel.: +49 711 685 83386, Fax: +49 711 685 83297
e-mail: firstname.secondname@ifp.uni-stuttgart.de
url: http://www.ifp.uni-stuttgart.de

Head of Institute

Director: Prof. Dr.-Ing. Dieter Fritsch
Deputy: apl. Prof. Dr.-Ing. Norbert Haala
Personal Assistant: Martina Kroma
Emeritus Professor: Prof. i.R. Dr. mult. Fritz Ackermann

Research Groups at the ifp:

Geoinformatics

Chair: Prof. Dr.-Ing. Dieter Fritsch
Deputy: Dr.-Ing. Volker Walter   Geographic Information Systems
Dr.-Ing. Susanne Becker   Point Cloud Interpretation and Hybrid GIS

Photogrammetry and Computer Vision

Chair: Prof. Dr.-Ing. Dieter Fritsch
Deputy: Dr.-Ing. Michael Cramer   Digital Airborne Sensors
Dr.-Ing. José Balsa-Barreiro   Cultural Heritage
Dipl.-Ing. Alessandro Cefalu   Photogrammetric Calibration and Object Recognition
M.A. Chance Michael Coughenour   Remote Sensing Applications to Archaeology
Dipl.-Ing.(FH) Markus Englich   Sensor Laboratory, Computing Facilities
MSc. Ke Gong   3D Reconstruction
MSc. Lavinia Runceanu   Modelling of Building Interiors

Photogrammetric Image Processing

Chair: apl. Prof. Dr.-Ing. Norbert Haala
MSc. Stefan Cavegn   Image-based Mobile Mapping
Dipl.-Ing. Patrick Tutzauer   Façade Reconstruction, Interpretation and Modelling

External Teaching Staff

Dipl.-Ing. Stefan Dvorak, Amt für Stadtentwicklung und Vermessung, Reutlingen

Research Projects

Geoinformatics

Understanding human perception of building categories in virtual 3D cities

Virtual 3D cities are becoming increasingly important as a means of visually communicating diverse urban-related information. Since humans are the direct recipients of this information transfer, it is vital that the 3D city representations account for the humans' spatial cognition. Thus, within project D01 „Perception-Guided Adaptive Modeling of 3D Virtual Cities" (SFB/Transregio 161), our long-term goal is providing a model for the effective perception-aware visual communication of urban- or building-related semantic information via geometric 3D building representations which induce a maximum degree of perceptual insight in the user's mind. A first step towards this goal is to get a deeper understanding of a human's cognitive experience of virtual 3D cities.

In this context, we developed and conducted a user study on the human ability to perceive building categories (*One-Family Building, Multi-Family Building, Residential Tower, Building With Shops - optionally with partial residential usage, Office Building, Industrial Facility*) from geometric 3D building representations. The category of a building is reflected in both geometric building properties (e.g. building size, roof shape, size, number and arrangement of windows etc.) and textural information. In order to separate the influences of both aspects as good as possible, the following three representation types are used within the study: (a) untextured LoD3 models for analyzing solely influences of geometric building and façade properties, (b) textured meshes/LoD2 models (from Google Earth) as well as images from Google Street View for analyzing influences of textural information. Figure 1 shows examples of the building categories and representation types presented to the user.

The study reveals various dependencies between geometric properties of the 3D representations and the perceptibility of the building categories. Knowledge about which geometries are relevant, helpful or obstructive for perceiving a specific building category is derived.

As a first application, we demonstrated how such knowledge about the human's perception of building-related semantic information can be used for the perceptually adapted abstraction of 3D building models. Characteristic properties of building structures that turned out to be essential for the perceptibility of a certain building category are maintained during the abstraction process whereas structures that are unimportant or even obstructive are simplified to a much higher extent or even totally neglected. As an example, Figure 2 (left) shows a detailed 3D façade model
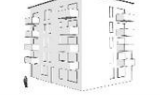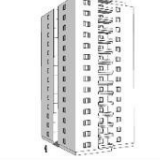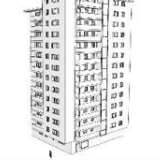
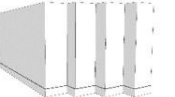|	LoD3 models				Textured Meshes (Google Earth)	Images (Street View)
One-Family Building (OFB)						
Multi-Family Building (MFB)						
Residential Tower (RT)						
Building With Shops (BWS)						
Office Building (OFF)						
Industrial Facility (IF)						

Figure 1: Examples for building categories and representation types used in the study (Google Earth/Street View, (C)2015 Google).

of a Residential Tower. Figure 2 (middle) depicts the result of a free abstraction without any restrictions. The result of the perception-aware abstraction can be seen in Figure 2 (right). Here, it has been considered that the occurrence of balconies is necessary for the user to distinguish the category Residential Tower from the category Office Building. Accordingly, the balconies have been maintained during the perception-aware abstraction process. Doing so, the perceptibility of the building category can be preserved even in the abstracted building representation.

Further tests will focus on user interaction with three dimensional data representations and classification results based on several parameters like viewing angle or architectural environment of the building of interest.
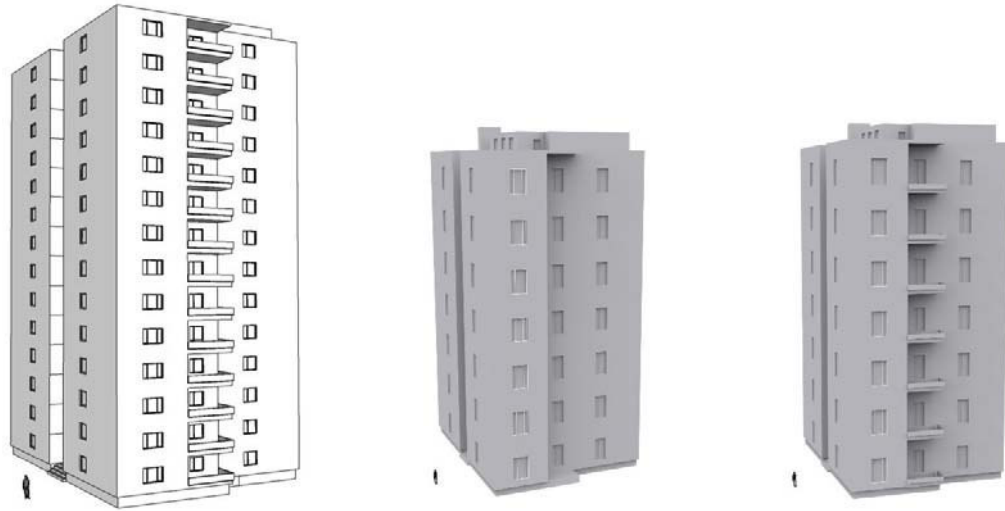
Figure 2: First application for conclusions drawn from the survey. Left: original building model; middle: 'free' abstraction without restrictions; right: abstraction based on features important for the user to classify into the respective correct category.

Use and Optimisation of Paid Crowdsourcing for the Collection of Geodata

Crowdsourcing is a new technology and a new business model that will change the way in which we work in many fields in the future. Employers divide and source out their work to a huge number of anonymous workers on the Internet. The division and outsourcing is not a trivial process but requires the definition of complete new workflows - from the definition of subtasks, to the execution and quality control. A popular crowdsourcing project in the field of collection of geodata is OpenStreetMap, which is based on the work of unpaid volunteers. Crowdsourcing projects that are based on the work of unpaid volunteers need an active community, whose members are convinced about the importance of the project and who have fun to collaborate. This can only be realized for some tasks. In the field of geodata collection many other tasks exist, which can in principle be solved with crowdsourcing, but where it is difficult to find a sufficient large number of volunteers. Other incentives must be provided in these cases, which can be monetary payments. The project described here has been realized with paid crowdsourcing, which means that the crowd-workers are paid for their work. We want to identify and quantify the parameters (e.g. amount of salary, size of working tiles or object types) which influence the quality of the results (especially: correctness, geometric accuracy and collection time).

We developed a web-based program for the collection of geodata and integrated it into the commercial crowdsourcing platform microWorkers (www.microWorkers.com), which takes over the recruitment and the payment. The platform has access to more than 600.000 registered crowdworkers. The workers are informed automatically when a new job is offered by an employer on the platform. The employers can restrict the jobs to specific groups of workers. For example, it is possible to offer the jobs only to workers that are living in a specific country or to workers that have already successfully worked on a particular number of other jobs. Further qualifications are possible with own developed tests, which must be solved before the job. After the job has been completed, the results are submitted to the employer who checks the quality of the results. The final payment is handled by the crowdsourcing platform.

A RGB orthophoto with a ground sampling distance (GSD) of 1m and a size of approximately 5*4 km^2 (see Figure 3) was subdivided into 88 patches with the size of 500 * 450m. Several campaigns with different parameters were launched on the microWorkers platform to evaluate the quality of the crowd-based data collection. All results were subdivided into five categories: Category 1 (very good): most of all data is correct collected (see example in Figure 4a); Category 2 (good): some objects are not collected, but overall the work has high accuracy (see example in Figure 4b); Category 3 (partly good): a significant amount of objects is not collected, but the remaining work is accomplished with high accuracy (see example in Figure 4c); Category 4 (poor): many objects are missing and the rest of the objects are collected with low accuracy (see example in Figure 4d) and Category 5 (unsatisfactory): the major area is not digitized (see example in Figure 4e) or the collected data is senseless (see example in Figure 4f).
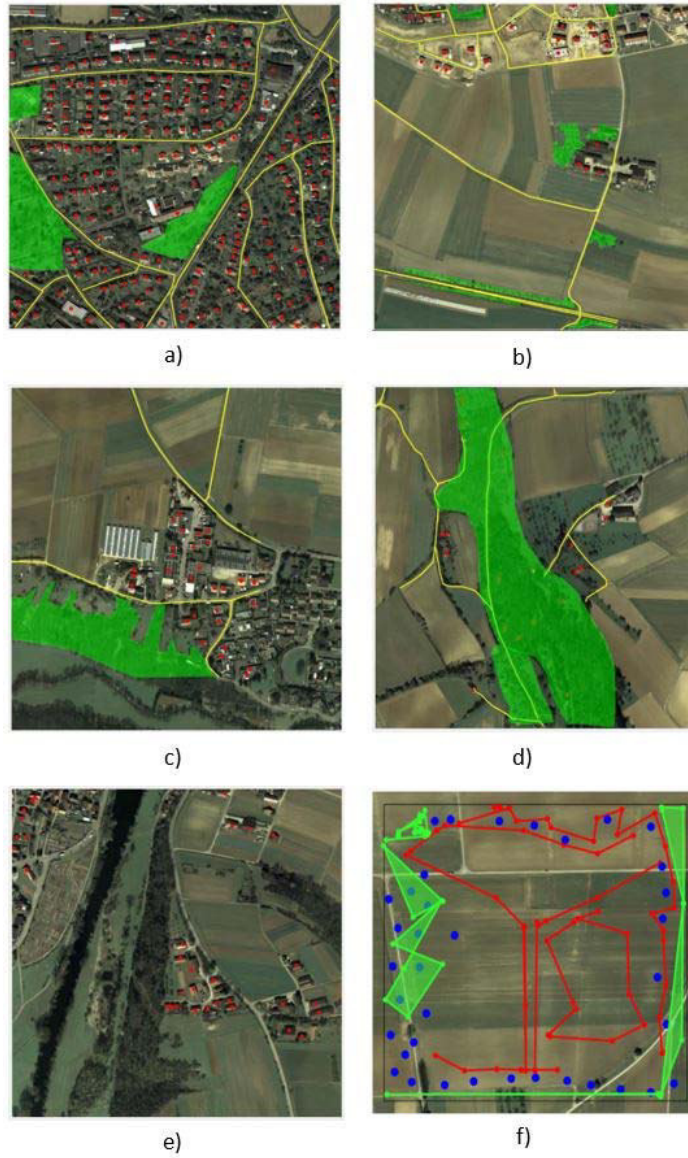

Figure 3: Test area

Figure 4: Examples of crowd-based spatial data collection,

The test showed, that most of all patches were collected with very good or good quality, but 10% to 20% of the patches were collected with lower quality. Therefore, it is necessary to find control mechanisms that evaluate the quality of the data. This either must be done automatically or again sourced out to the crowd. Furthermore, selection procedures are needed, which can automatically select crowd-workers who collect data with high quality. This can be realized for example with user profiles. Finally, algorithms are needed which integrate the individual results into an overall result. Spatial inconsistent datasets, which overlap multiply, have to be integrated into a consistent, uniform dataset. All these aspects will be investigated in our ongoing research.

Photogrammetry and Computer Vision

Crowd-sourced Indoor Modelling

Humans spend most of their time indoors and need location based facilities, especially in public buildings. However, a large amount of indoor space is unmapped. The increasing availability of powerful mobile devices, like smartphones and tablets, motivates the use of crowd-sourced data, such as images, videos or point clouds, to model the 3D indoor space.

Considering that the input data is coming from different sources and that it may be noisy and incomplete, it is neccessary to develop a robust algorithm which makes use of an interior grammar capable to describe 3D structures and semantic information. An important feature of the grammar should be its capability of learning and predicting semantic information.

Knowing that most of the public buildings contain spaces with poor texture, first investigations with a depth sensor, Google Project Tango, were done. The resulting point cloud was passed through a processing pipeline for removing the noise and obtaining a suitable input for the interior grammar. A sample of a point cloud collected with Project Tango and the resulting orthographic image is shown in Figure 5.

Figure 5: Left: Raw point cloud from Project Tango; Right: Orthographic projected image.

3D Reconstruction with High Resolution Satellite Data

Since satellite sensors can provide panchromatic imagery with half meter or even better resolution, high resolution satellites (HRS) have become an important data source for many photogrammetric tasks. HRS images have the advantage that they provide a very detailed view of the landscape and have a much larger coverage than images from aerial photogrammetry. The present work aims at building a robust automatic pipeline to produce DSMs from HRS stereo imagery. The satellite images were collected by Worldview-1 with 0.5m GSD from the three testsites La Mola, Terrassa and Vacarisses in Catalonia, Spain. The pipeline consists of the follwoing steps:

▷ Bundle adjustment: This step applies the Rational Polynomial Coefficients (RPCs) provided by the satellite venders to compute the exterior orientation. An additional affine model is used for bias compensation.

▷ Image rectification: This step builds the epipolar geometry of the satellite imagery by Projection-Trajectory based epipolarity (PTE) model and then resamples the rectified images. The bias-compensated RPCs are applied to build the projection relationship between the image and object space. The vertical parallaxes in the rectified image pair are in sub-pixel level.

▷ Dense image matching: The C++ library LibTsgm, which is provided by nFrames GmbH, is applied for this procedure. A Semi-Global Matching procedure processes the image pair pixel by pixel and produces a disparity image.

▷ Triangulation: According to the bias-compensated RPCs, the point cloud is calculated by forward intersection. Finally, a DSM is generated from the point cloud.

The final point clouds are presented in Figure 6. The distribution of the elevation shift is depicted as histogram for each testsite (Figure 7). Median and the normalized median deviation (NMAD) are selected as the mean height difference and standard deviation of robustness estimation. Here, 68% and 95% quantiles of absolute error are also taken into consideration. Table 1 shows the statistic evaluation for all three testsite. The reference data is a LIDAR point cloud with 1m GSD. The results indicate that the DSM has acceptable precision and robustness.

Testsite	Mean (m)	Std (m)	RMSE (m)	Median (m)	NMAD (m)	Aq68 (m)	Aq95 (m)
La mola	-0.32	2.71	2.73	-0.18	1.16	1.41	6.39
Terrassa	0.14	1.34	1.34	0.17	0.57	0.70	3.14
Vacarisses	-0.03	2.77	2.77	-0.10	1.45	1.81	6.65

Table 1: Statistic evaluation of Worldview-1 and LIDAR reference DSM.
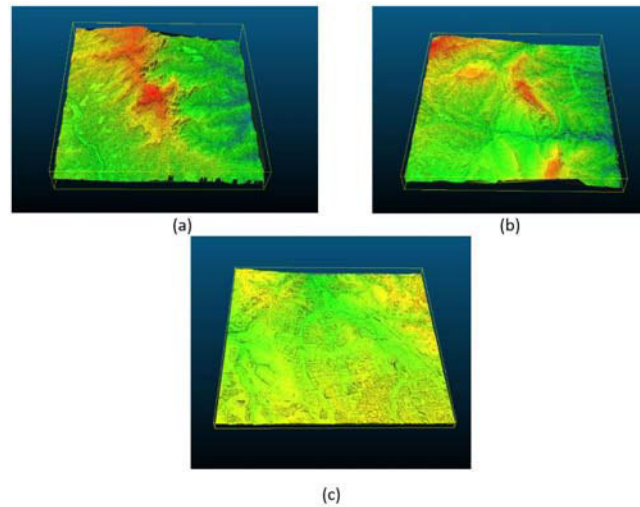
Figure 6: Point clouds generated from Worldview-1 data: (a) La Mola (b) Vacarisses (c) Terrassa
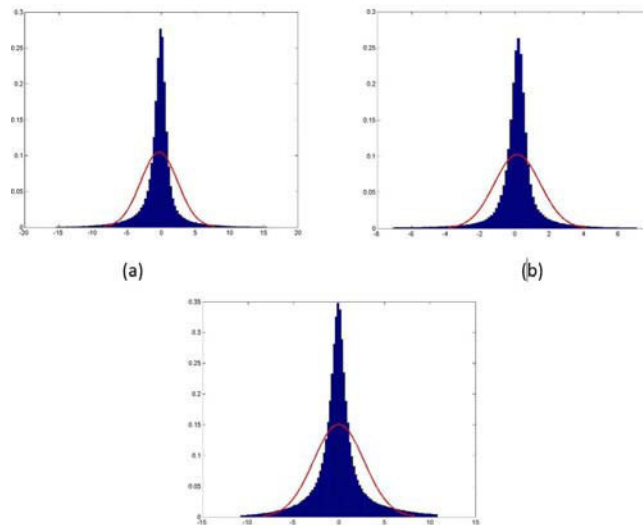

Figure 7: The red curves are the expected distribution according to the normal distribution with the calculated mean and standard deviation.

Integrating Laser Scanning and Computer Vision in Mesoamerican Archaeology

The importance of increasing topographic and geometric information of archaeological sites continues to advance thanks to developments in disciplines such as geodesy and computer vision. Archaeological investigations can benefit considerably by intensively increasing the amount of data collected for purposes of 2D, 3D, and 4D geometric documentation. During the 2015 field season, the University of Bonn collaborated with the ifp to realise an acquisition campaign from 8 April to 3 May at the ancient Maya city of Uxul in the dense jungle of the Calakmul Biosphere in southern Mexico. Field acquisition was completed with the FARO Focus 3D X130 laser scanner and two Canon EO5-5D Mark II calibrated cameras.

Three architectural groups were documented using both active and passive sensors in order to achieve an integrated result with previously acquired topographic and excavation data. Smaller cultural remains, some with painted text and iconography, were also documented using photogrammetry at various museums and project storage facilities in order to digitally reconstitute these objects in situ. Due to thick vegetation and unstable architectural remains, photogrammetry was also found as a solution to reach structural locations not possible with the laser scanner. The humid, tropical environment provided a number of challenges to the project, especially when working with sensitive equipment. Nevertheless, the field campaign was successful.
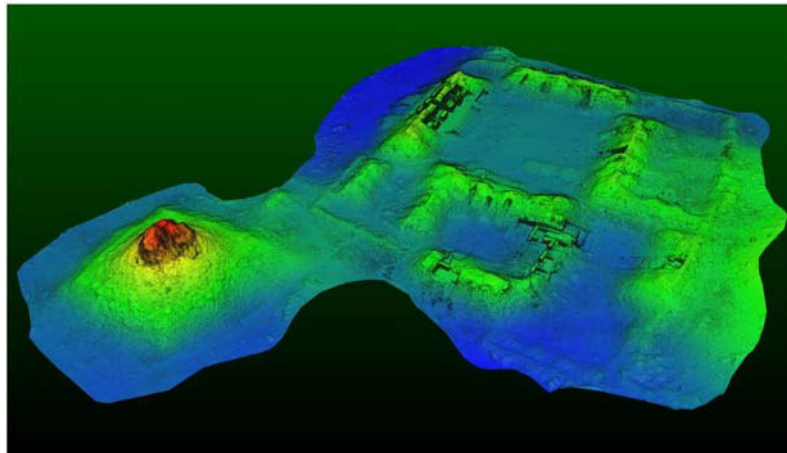
Figure 8: Digital Terrain Model of Group K from terrestrial acquisition.

In comparison to traditional land surveying methods, laser scanning and computer vision can greatly augment archaeological survey and investigation. Data processing has been carried out both in Stuttgart and in Bonn in order to intensively investigate and digitally preserve the ancient engineered landscape of the site. Deformations to architecture caused by erosion and vegetation

can be more thoroughly measured for understanding construction phases and facilitate 3D reconstruction modelling. By segmenting the vegetation from the terrain and architectural remains, these data additionally provide multidisciplinary research into ancient hydrology and contemporary botany. Small-scale data integration will also contribute to new epigraphic understanding and virtual investigations of their temporal and spatial contexts. Such examples of non-invasive techniques offer new possibilities to the field of archaeology, especially since traditional excavation methods in essence are destructive by their very nature. The results of this project will be interactively exhibited at museum exhibitions at the History Museum in Speyer, Germany and the Drents Museum of Assen in the Netherlands in 2016.
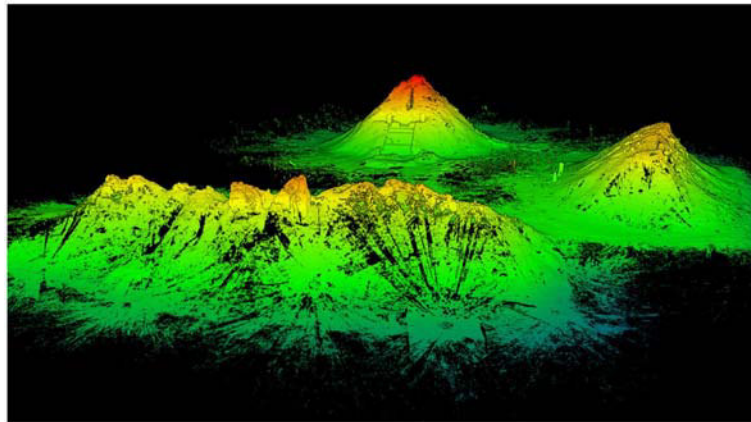

Figure 9: Point cloud with vegetation segmented of Group D.

4D Cultural Heritage World

The project *4D Cultural Heritage World* is focused in the fast and cost-effective reconstruction using images obtained in the wild. This project supports the aim of European Commons and the digital libraries *Europeana* and *Unesco Memory of the World* to build a sense of a shared European cultural history and identity.

The project develops a fully automated time-varying 3D model engine for cultural heritage urban environments from a large collection of historical images, enabling to access and retrieve of high quality content but also supporting more sophisticated functionalities such as interoperable cultural object descriptions, immersion of content into diverse contexts, 3D reconstruction of damaged artifacts, etc. This project forms the basis for studying, understanding, preserving and documenting urban environments, as well as organizing collections of thousands of images (spatially and temporally). The final models enable to get novel views of historical scenes by interacting with the time varying model itself.
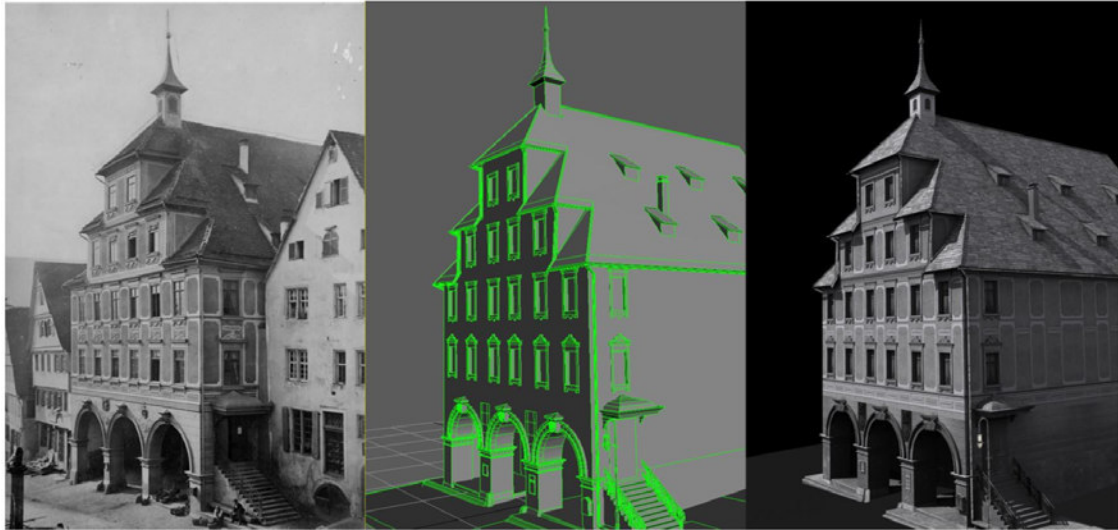
Figure 10: Reconstruction of the Town Hall of Calw.

The testbed area chosen for this project is the historical city of Calw, next to Stuttgart. This city has a relevant history and preserves still a rich architectural heritage.

Several students of the Master Program *Geoengine* are involved in the generation of 3D photorealistic models of some of the most representative buildings of Calw. At the moment, eight students have collaborated (five of them during the current course 2015-2016), which have reconstructed around 100 buildings in their Master's Thesis.

Photogrammetry, laser scanner and computer vision are used for the reconstruction of the buildings. The laser measurements are carried out with terrestrial laser systems from static and fixed positions. These measurements enable to draw an accurate geometric representation of the objects scanned. The texture information of the building are incorporated from the images collected, previously arranged and prepared.

The results obtained are incorporated and integrated into an app (Calw VR.app), in which the user can immerse into the virtual environment of the Calw city. Thus, the user can display the actual 3D model besides to the virtual recreation of the past. The expansion of the studied area, the improvement and the incorporation of new functionalities to this app are the next challenges for the next months.

Figure 11: Screenshot of the market place of Calw obtained in the application Calw VR.app.

Non-Incremental Structure from Motion with Structureless Bundle Adjustment

The majority of approaches to Structure from Motion (SfM) apply an incremental triangulate-and-resect strategy in order to reconstruct camera motion and scene structure in a common reference frame. The sequential addition of images may cause a drifting behavior during the reconstruction, in some cases causing the process to fail. Usually, within SfM, classical bundle adjustment (BA) based on collinearity is applied to optimize intermediate and final results of the process. Next to the cameras' orientations and intrinsic parameters it involves the 3D coordinates of observed scene points, which results in a nonlinear system with a large number of unknowns.

Over the last decade, more attention has come to non-incremental approaches to SfM, which exploit the network characteristics arising from 2-, 3- or n-view relations, given for a set of images through relative orientations. Usual approaches employ an initial removal of outlier connectivities based on rotational loop consistency, followed by rotation registration and finally, translation registration. The latter can be carried out without scene reconstruction. To achieve higher robustness, it has been suggested to use triplets of images in this step. We build on this approach and augment it by an additional step, using submodels with (arbitrary) higher image numbers. This results in less drift in scale and orientation, which may occur with unstable camera station distribution and unknown camera calibration.

Additionally, we replace classical BA by structureless bundle adjustment. The term refers to methods mainly relying on the epipolar constraint, which does not involve the object space coordinates of observed points. However, for the epipolar constraint, collinear camera stations form a degenerate case. The cameras can be positioned on the line, but the distances between the cameras

remain ambiguous. In order to overcome this problem, additional scale consistency constraints may be applied to threefold (or higher) observations. Although the number of unknowns is drastically reduced, the number of equations arising within the structureless approaches easily exceeds that of classical BA. This fact is usually only met by neglecting some of the available redundancy.
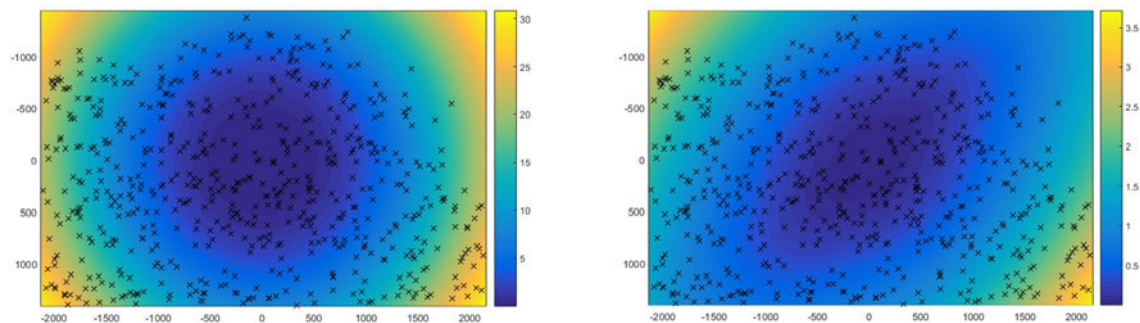

Figure 12: Exemplary result of camera calibration using our approach. Magnitude of image distortion in pixel units. Left: radial distortion, right: tangential distortion. The crosses indicate the overall distribution of observations.

Our approach differs in the following points, which to our knowledge have not been suggested before. We have developed a scale consistency constraint based on the law of sines which minimizes triangulation errors in object space. Furthermore, we reformulate the constraints, to include distortion parameters (Brown model). This enables us to use the structureless approach for (simultaneous) camera calibration. Finally, we suggest accumulating constraints, in order to reduce the memory footprint of the Jacobian. The resulting number of equation equals that of classical BA.

The whole resulting SfM process chain entirely avoids 3D structure computation, instead only camera orientation and intrinsic parameters are computed. Surface reconstruction (Figure 13) is, if needed, carried out as a final and fully decoupled step.

Directly measured GNSS/Inertial exterior Orientations for UAS Corridor Surveys

The use of unmanned aircraft systems (UAS) for photogrammetric data collection to derive 3D point clouds and orthophotos seems to be established. Latest commercial, so-called inspection drones were presented, which in theory should allow to collect 3D data with very high resolution and accuracy. This opens a new application field which previously was reserved for engineering geodesy only. Obviously there is a certain demand for very high accuracy (engineering) applications up to the sub-centimeter or even millimeter accuracy range. It could be applications like the survey of linear objects such as river or canal bank. Here, very precise UAS-photogrammetry
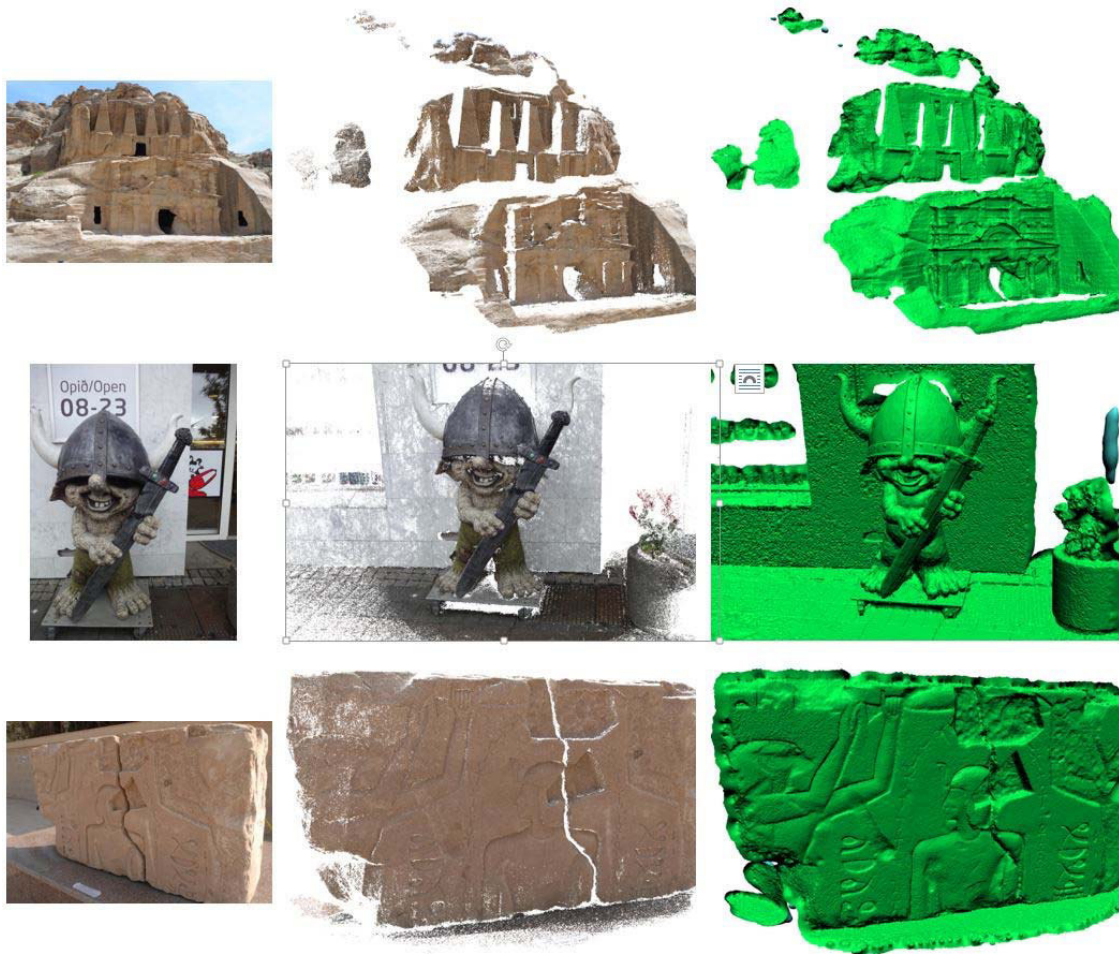
Figure 13: Visual impressions of resulting surface reconstructions. From left to right: example image, dense point cloud, meshed surface with normal shading.

may help to detect riverside deformations in the terrain shape, in order to prevent major terrain slides. In addition to the high requirements in terms of accuracy, the survey of such linear objects additionally suffers from their elongated dimension which particularly has an influence on the subsequent aerial triangulation. Strip-wise or linear image blocks (linear photogrammetry) suffer from block geometry, especially if only a limited number of reference data is available on the ground. The only way to overcome this is the additional use of directly measured elements of the exterior

orientation (EO) from integrated GNSS / inertial systems. Such high precision integrated systems are now available for use in lightweight UAS with high accuracy. Their expected accuracy should be in the range of 2-5cm for position and 0.025-0.08deg for attitude.

Extensive simulations have been made to investigate the use of directly measured GNSS/inertial in photogrammetric processing of linear objects. The focus is on simulation of strip-shaped image blocks to investigate the influence for such UAS image corridor evaluation. Different to classical aerial surveys nadir imagery was combined with slightly tilted camera views, as it can be easily realized by multi-copter platforms with gimballed camera mount. With that, base lines perpendicular to the flight direction can be realized, even though images cover the same area, i.e. the small strip of open terrain right close to the river bank.

Simulation has shown that with such combined forward and tilted overlapping imagery and the use of high performance GNSS/inertial direct exterior orientation elements, long strips with more than 350 images can be bridged without any ground control. The precision stays constant within the expected and desired quality range and is fully controlled through the overlap and the directly measured EO parameters (see Figure 14). In addition, the precision of image point measurement also is of influence. In order to get highest accuracy the tie point extraction from SIFT should to be refined by least-squares matching.

Besides the quality of the sensor orientation and image point measurements the performance of the camera system and its overall system integration is crucial, especially for those direct geo-referencing approaches. Engineering applications require very high resolutions (a few millimeter) in the object space and therefore accuracy. But accuracy is also linked to the camera resolution, i.e. precise point definitions are only possibly in highly resolved images. This directly leads to the question whether the existing UAS-cameras can deliver this accuracy, or whether there is a demand for a specific UAS-based mapping camera there? The performance of typical (off-the-shelf) camera systems often used in such UAS-scenarios has to be further analyzed where especially the kinematic scenarios are interest. The influence of platform movements and vibration effects, which often play a role in (multi-rotor) UAS-platforms, may influence image quality and thus its resolution.
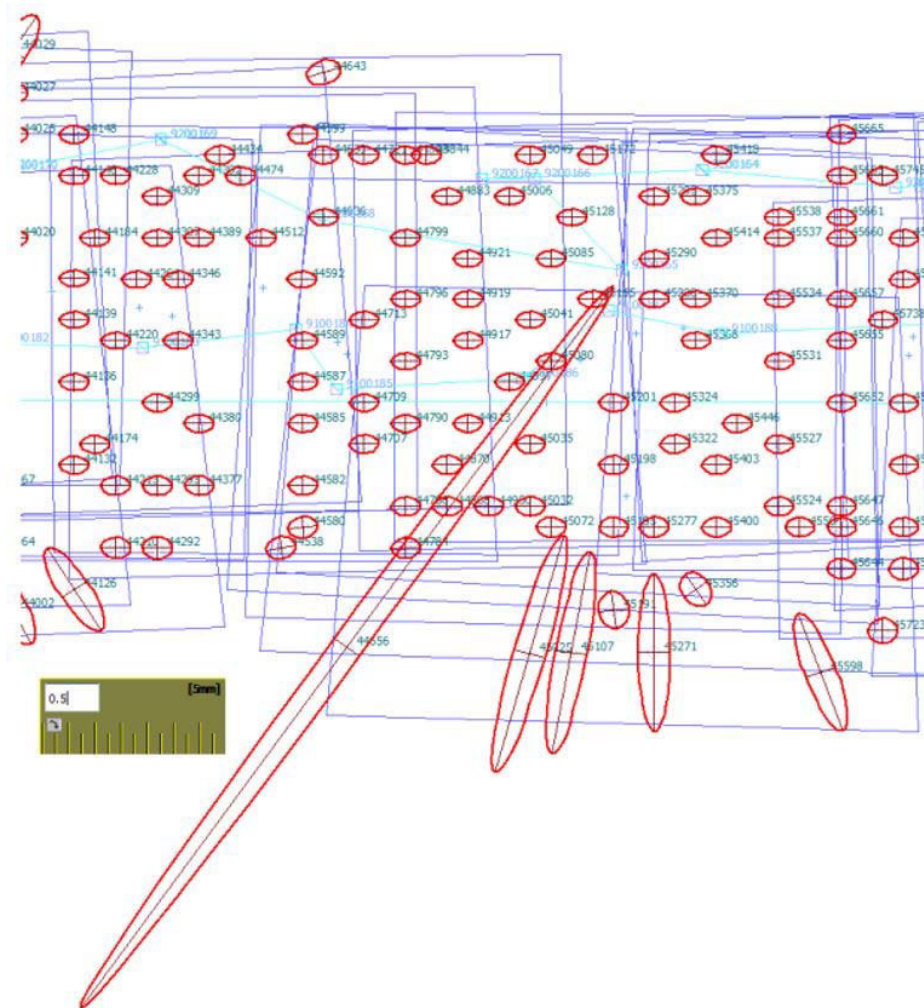
Figure 14: (Horizontal) error ellipses in the center of a 350 images long strip from simulation. The ellipses are close to circles, the precision perpendicular to flight direction is slightly better than in flight direction, which shows the high impact of the EO observations. Some only two folded object points at the borders of the strip show worse precision due to the intersection geometry, but they have no influence for the later practical projects.

Photogrammetric Image Processing

Image-based mobile Mapping for 3D urban Data Collection

In order to achieve highest resolution and accuracy of 3D object reconstruction in complex urban environments, data collection from terrestrial viewpoints is still required in addition to oblique airborne imagery. Such area covering terrestrial data collection can be realized efficiently by street-level mobile mapping. Frequently, these systems use LiDAR sensors to provide 3D point clouds for applications like road management or rural and urban structuring. Meanwhile, the progress in dense multi-stereo image matching enables 3D data collection using camera-based systems as a suitable alternative.

In order to demonstrate the potential, stereo imagery was collected every meter by the multi-view multi-sensor stereovision mobile mapping system of the Institute of Geomatics Engineering (IVGI), University of Applied Sciences and Arts Northwestern Switzerland (FHNW) at a very busy junction of five roads in the city center of Basel in July 2014. Although three stereovision systems are available (see Figure 15), the main stereo system facing forward always features the highest resolution and hence accuracy potential.

Figure 15: Sensor configuration of the multi-view stereovision IVGI mobile mapping system.

For processing and investigations of mobile mapping image sequences, the two matching configurations c1 and c4 depicted in Figure 16 were selected. While configuration 1 represents standard stereo matching with one base and one match image collection at the same point of time, configuration 4 additionally incorporates matching with the two previous and the two following images resulting in five neighboring match images. This redundancy should lead to an increase in completeness, reliability and accuracy.

Forward, back-right and left stereo imagery was processed by the stereo-matching-software SURE exploiting configurations 1 and 4. The resulting point clouds were filtered using an octree based approach. Aiming at generating a dense scene in object space, high density and good coverage on the sidewalks and façades for the forward stereovision system was achieved. However, this also caused some clutter especially around overhead wires and a considerable number of points representing moving objects were not removed like the tramway in the middle of Figure 17.
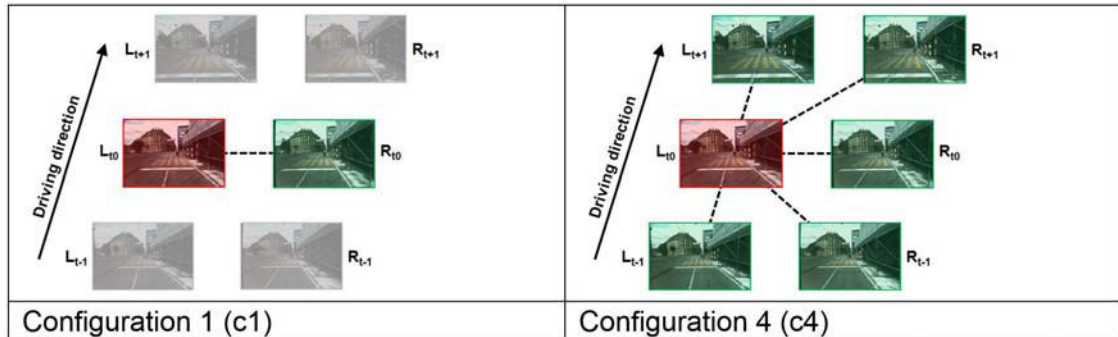
Figure 16: Selected matching configurations, red: base image, green: match images.

Figure 17: Filtered point cloud generated by incorporating forward stereo imagery and exploiting five match images per base image (c4).

In order to carry out some numerical investigations, density as well as deviation values between dense image matching and terrestrial laserscanning point clouds for several predominantly planar road patches were determined.

In terms of density, large values were computed for both c1 and c4 for the back-right (ca. 16,000 points/) in contrast to the forward stereovision system where density values are approximately three times larger for c1 than for c4 (ca. 23,000 vs. ca. 7,500 points/m^2). However, density is highly dependent on filtering parameters and especially on the filtering degree.

Slightly higher accuracy values could be determined for c4 (mean RMSE 22-27 mm) than for c1 (mean RMSE 26-33 mm) which is caused by the higher redundancy of c4. Mainly due to large distances between the stereo cameras and the respective patches, the left stereovision system provides the less accurate patches. Similar accuracies were determined for the back-right and forward patches as the lower resolution of the back-right compared to the forward stereovision system is compensated by shorter distances to the patches.

Investigations clearly demonstrated the benefit of exploiting imagery from the back-right and left stereovision systems in addition to forward especially for sidewalk and lower façade areas. Even for challenging scenarios, dense image matching provides high quality point clouds and depth information for almost every pixel.

References 2015

Balsa-Barreiro, J., Fritsch, D.: Generation of 3D/4D Photorealistic Building Models. The Testbed Area for 4D Cultural Heritage World Project: The Historical Center of Calw (Germany). In: 11th International Symposium on Visual Computing (ISVC), Dec 14-16, 2015, Las Vegas.

Becker, S., Peter, M., Fritsch, D.: Grammar Supported 3D Indoor Reconstruction From Point Clouds For „As-built" BIM. In: ISPRS Ann. Photogramm. Remote Sens. Spatial Inf. Sci., II-3/W4, 17-24.

Cavegn, S., Haala, N., Nebiker, S., Rothermel, M., Zwölfer, T.: Evaluation of Matching Strategies for Image-Based Mobile Mapping. ISPRS Annals Vol II-3/W5, 361-368.

Coughenour, C.M., Vincent, M.L., de Kramer, M., Senecal, S., Fritsch, D., Guiterrez, M.F., Lopez-Menchero Bendicho, V.M., Ioannides, M.: Embedding Knowledge in 3D Data Frameworks in Cultural Heritage. In: ISPRS Ann. Photogramm. Remote Sens. Spatial Inf. Sci., II-5/W3, 47-52.

Coughenour, C., Fritsch, D.: The Marie Sklodowska-Curie ITN-DCH Project - Overview and Scientific Work. In: Fritsch, D. (Ed.): Photogrammetric Week 15, Wichmann/VDE Verlag, Berlin, Offenbach, 65-71.

Fritsch, D., Syll, M.: Photogrammetric 3D Reconstruction Using Mobile Imaging. in: SPIE Proceedings, IS&T Electronic Imaging, Vol. 9411, 15p.

Fritsch, D.: Some Stuttgart Highlights of Photogrammetry and Remote Sensing. In: Fritsch, D. (Ed.): Photogrammetric Week 15, Wichmann/VDE Verlag, Berlin, Offenbach, 3-20.

Fritsch, D. (Ed.): Photogrammetric Week '15. Proceedings. Wichmann/VDE Verlag, Berlin, Offenbach, 394p.

Fritsch, D.: Photogrammetrische Auswertung digitaler Bilder - Neue Methoden der Kamerakalibration, dichten Bildzuordnung und Interpretation von Punktwolken. Rummel, R., Freden, W. (Eds): Handbuch der Geodäsie, 30p.

Fritsch, D.: Ausgleichungsrechnung damals und heute. In: Baumann, E. (Ed.): Johann Gottlieb Friedrich Bohnenberger, Verlag W. Kohlhammer, Stuttgart.

Fritsch, D.: Punktwolken, und was dann? vgi, Österreichische Zeitschrift für Vermessung und Geoinformation, Heft 1/2015, 54-66.

Haala, N., Cavegn, S.: Benchmark zur Evaluation dichter Bildzuordnungsverfahren in Luftbildern. In: Jahrestagung DGPF, Tagungsband 24, 244-253.

Haala, N., Rothermel, M.: Image-based 3D Data Capture in Urban Scenarios. In: Photogrammetric Week '15. Ed. D. Fritsch, Wichmann/VDE Verlag, Berlin, Offenbach, 119-130.

Haala, N., Rothermel, M., Cavegn, S.: Extracting 3D Urban Models from Oblique Aerial Images. In: JURSE 2015 Joint Urban Remote Sensing Event, Lausanne, Switzerland, 4p.

Haala, N., Tutzauer, P., Becker, S.: Automatisierte Erzeugung von LOD3-Modellen aus 3D-Punktwolken durch Multi-Stereo-Bildzuordnung. In: Geoinformationssysteme 2015, Beiträge zur 2. Münchner GI-Runde, Wichmann/VDE Verlag, Berlin, Offenbach, 108-119.

Ioannides, M., Alexakis, E., Coughenour, C.M., Vincent, M.L., Guiterrez, M.F., Lopez-Menchero Bendicho, V.M., Fritsch, D., Moropoulu, A., Rajcic, V., Zarnic, R.: Digital Cultural Hertitage - A Challenge for the Chemical Engineering: Contextualizing Materials in a Holistic Framework. In: Proceedings ETNDT6 Conference.

Vincent, M.L., Coghenour, C.M., Remondino, F., Flores Guiterrez, M., Lopez-Menchero Bendicho, V.M., Fritsch, D.: Crowd-sourcing the 3D Digital Reconstructions of Lost Cultural Heritage. In: Proceedings Digital Heritage, Grenada.

Tutzauer, P., Haala, N.: Facade Reconstruction Using Geometric and Radiometric Point Cloud Information. In: ISPRS Ann. Photogramm. Remote Sens. Spatial Inf. Sci., XL-3/W2, 247-252.

Walter, V., Laupheimer, D., Fritsch, D.: Use of Paid Crowdsourcing for the Collection of Geodata. In: 1st ICA European Symposium on Cartography, Vienna, 6p.

Master Theses

Garoiu, L.: Theoretical and empirical investigations of oblique airborne image geometry. Supervisors: Gruber, M. (Microsoft Vexcel Imaging), Cramer, M.

Dejan, D.: Development of an Android-based app for the management of communal geoinformation. Supervisor: Walter, V.

Erikipati, M.: Implementation and comparison of content based image retrieval methods. Supervisor: Walter, V.

Heck, C.: Performance of Precise GNSS/Inertial Trajectory Solutions in UAS Photogrammetry. Supervisors: Heuchel, T. (Trimble Germany, Geospatial Division), Cramer, M.

Xie, D.: Untersuchung von PnP-Algorithmen für photogrammetrische Anwendungen. Supervisors: Heuchel, T. (Trimble Germany, Geospatial Division), Haala, N.

Fang, M.: Schätzung der Posen bewegter Kameras mit Hilfe von Landmarken. Supervisors: Kühnle, J. (Fraunhofer/IPA), Haala, N.

Wang, Y.: Digital Preservation of Calw Lederstrasse Using Terrestrial Laser Scanning and Photogrammetry. Supervisor: Fritsch, D.

Yanteng, J.: Digital Preservation of Calw Market Square - Lederstrasse by Means of Automated HDS and Phtotgrammetric Textur Mapping. Supervisor: Fritsch, D.

Bachelor Theses

De Keersmacker, J.: Entwicklung einer GUI zur Darstellung von raumbezogenen Zugriffsverfahren. Supervisor: Walter, V.

Schneider, P.: Automatische Erkennung von Gebäudeinfrastrukturelementen in Sensordaten des Project Tango Tablets. Supervisors: Schneider, M., Haala, N.

Schmidt, J.: Photogrammetrische Rekonstruktion historischer Krippenfiguren. Supervisors: Cramer, M., Haala, N.

Grellmann, A: Erstellung einer GUI zur Auswertung von CBIR-Verfahren. Supervisor: Walter, V.

Sulzer, R.: Photogrammetrische Schneehöhenbestimmung mit einer UAV-Plattform. Supervisor: Haala, N.

Foof, S.: Untersuchung zur flächenhaften Erfassung von Schneehöhen durch terrestrische Photogrammetrie und Laserscanning. Supervisor: Cefalu, A.

Pang, H.: Generierung dichter Punktwolken mit UAS-Software - Empirische Genauigkeitsuntersuchung. Supervisor: Cramer, M.

Han, M.: Qualitätsuntersuchung von 3D-Punktwolken aus Schrägluftbildern. Supervisor: Haala, N.

Wu, S.: Automatische Rekonstruktion von Fassadenstrukturen aus 3D-Punktwolken. Supervisor: Becker, S.

Weimann, D.: Virtuelle Grenzlagenvisualisierung. Supervisor: Fritsch, D.

Paschke, M.: Erfassung und Charakterisierung des Kraftstoffsprays von Hochdruckeinspritzventilen für Benzindirekteinspritzung. Supervisor: Fritsch, D.

Activities in National and International Organizations

Cramer, M.:
Co-Chair ISPRS ICWG III/I: Sensor Modeling for Integrated Orientation and Navigation

Englich, M.:
Webmaster ISPRS

Fritsch, D.:
Chairman Board of Trustees 'The ISPRS Foundation'
Member CyberOne Award Commitee
Member Galileo/GMES Award Committee Baden-Württemberg
Member Jury Artur Fischer Invention Award
Member D21 Advisory Board
Member Board of Trustees German University in Cairo (GUC)
Member GUC Academic Advisory Committee
Member GUC Academic Promotion Commitee
Member Apple's University Education Forum (UEF)
Member Scientific Advisory Board CoE LaSR, Helsinki, Finland
Reviewer Academy of Finnland
SUSTECH Visiting Professor, Khartoum
GUC Visiting Professor, Cairo

Haala, N.:
Chair ISPRS WG I/2 - LiDAR, SAR and Optical Sensors
Vorsitz DGPF Arbeitskreis Sensorik und Plattformen

Walter, V.:
Member Editorial Advisory Board ISPRS Journal of Photogrammetry and Remote Sensing
Nationaler Berichterstatter für die ISPRS Kommission IV

Education - Lectures/Exercises/Training/Seminars

Bachelor „Geodäsie und Geoinformatik"

Adjustment Theory I (Fritsch, Sneeuw)	1/1/0/0
Adjustment Theory II (Fritsch, Sneeuw)	2/2/0/0
Geoinformatics I (Fritsch, Walter)	2/2/0/0
Geoinformatics II (Walter)	1/1/0/0
Image Processing (Haala)	2/1/0/0
Integrated Fieldworks (Fritsch, Sneeuw, Keller, Kleusberg)	0/0/4/0
Introduction into Geodesy and Geoinformatics (Cramer, Fritsch, Sneeuw, Keller, Kleusberg)	4/2/0/0
Photogrammetry (Cramer)	2/1/0/0

Signal Processing (Fritsch) · 2/1/0/0

Urban Planning (Dvorak) · 2/0/0/0

Master Course „Geodäsie und Geoinformatik"

Aerotriangulation (Cramer) · 1/1/0/0

Close Range Photogrammetry and Machine Vision (Fritsch) · 1/1/0/0

Computational Geometry (Walter) · 1/1/0/0

Computer Vision for Image-based Acquisition of Geodata (Haala) · 1/1/0/0

Databases and Geographical Information Systems (Walter) · 1/1/0/0

Digital Terrain Models (Haala) · 1/1/0/0

Fundamentals in Urban Planning (Dvorak) · 2/0/0/0

Georeferencing of photogrammetric Systems (Cramer) · 1/1/0/0

Modelling and Visualisation (Haala) · 1/1/0/0

Pattern Recognition and Image Understanding (Haala) · 1/1/0/0

Scientific Presentation Seminar (Haala) · 0/0/0/2

Terrestrial Laserscanning (Fritsch) · 1/1/0/0

Topology and Optimisation (Becker) · 1/1/0/0

Web-based GIS (Walter) · 1/1/0/0

Master Course GEOENGINE

Airborne Data Acquisition (Fritsch, Cramer) · 2/1/0/0

Geoinformatics (Fritsch, Walter) · 2/1/0/0

Signal Processing (Fritsch) · 2/1/0/0

Topology and Optimisation (Becker) · 2/1/0/0

Image-based Data Collection (Fritsch, Cramer) · 2/1/0/0

Integrated Fieldworks (Fritsch, Sneeuw, Keller, Kleusberg) · 0/0/4/0

Master Course „Infrastructure Planning"

Introduction to GIS (Walter) · 2/0/0/0

Master Course „Aerospace Engineering"

Image Processing (Haala) · 2/1/0/0

Introduction into projective Geometry (Cramer) · 2/0/0/0

Optical Remote Sensing (Fritsch) · 2/0/0/0